

1 **LARGE-SCALE BIOLOGY ARTICLE**

2 **A PXY-Mediated Transcriptional Network Integrates Signaling**
3 **Mechanisms to Control Vascular Development in Arabidopsis**

4
5 **Margot E. Smit^{1,2,3}•, Shauni McGregor^{4,5}•, Heng Sun⁶, Catherine Gough⁴, Anne-Maarit**
6 **Bågman¹, Cara L. Soyars^{7,8}, Johannes T. Kroon⁴, Allison Gaudinier^{1,9}, Clara J.**
7 **Williams^{1,10}, Xiyan Yang⁶, Zachary L. Nimchuk⁷, Dolf Weijers², Simon R. Turner¹¹,**
8 **Siobhán M. Brady*¹ and J. Peter Etchells*^{1,4}**

9
10 ¹ University of California Davis, Plant Biology & Genome Center, Davis, California, 95616,
11 USA

12 ² Laboratory of Biochemistry, Wageningen University, the Netherlands.

13 ³ Stanford University, Stanford, CA, USA, 94305-5020

14 ⁴ Durham University, Department of Biosciences, Durham, DH1 3LE, UK

15 ⁵ Current address: University of Sheffield, APS, Western Bank

16 ⁶ National Key Laboratory of Crop Genetic Improvement, Huazhong Agricultural University,
17 Wuhan, Hubei, 430070, PR China

18 ⁷ Department of Biology, University of North Carolina at Chapel Hill, Chapel Hill, North
19 Carolina, USA.

20 ⁸ Thermo Fisher Scientific

21 ⁹ Department of Plant and Microbial Biology, University of California Berkeley, CA 94720,
22 USA

23 ¹⁰ Current address: UGhent, VIB Department of Plant Systems Biology, Belgium.

24 ¹¹ University of Manchester, Faculty of Life Sciences, Manchester, M13 9PT, UK.

25 • Equal contribution

26 *Corresponding authors: Peter.Etchells@durham.ac.uk; sbrady@ucdavis.edu

27
28 **Short title:** An Arabidopsis vascular development network

29
30 **One sentence summary:** A feed-forward loop that controls vascular development was
31 uncovered by identifying a transcriptional network mediated by the receptor kinase
32 PHLOEM INTERCALATED WITH XYLEM.

33
34 The authors responsible for distribution of materials integral to the findings in this article in
35 accordance with the policy described in the instructions for authors (www.plantcell.org) are J.
36 Peter Etchells (Peter.Etchells@durham.ac.uk) and Siobhán M. Brady (sbrady@ucdavis.edu)

37
38 **ABSTRACT**

39 The cambium and procambium generate the majority of biomass in vascular plants. These
40 meristems constitute a bifacial stem cell population from which xylem and phloem are
41 specified on opposing sides by positional signals. The PHLOEM INTERCALATED WITH
42 XYLEM (PXY) receptor kinase promotes vascular cell division and organisation. However,
43 how these functions are specified and integrated is unknown. Here, we mapped a putative

44 PXY-mediated transcriptional regulatory network comprising 690 transcription factor-
45 promoter interactions in *Arabidopsis thaliana* (Arabidopsis). Among these interactions was a
46 feed-forward loop containing transcription factors WUSCHEL HOMEODOMAIN RELATED14
47 (WOX14) and TARGET OF MONOPTEROS6 (TMO6), which each regulate the expression
48 of the gene encoding a third transcription factor, LATERAL ORGAN BOUNDARIES
49 DOMAIN4 (LBD4). PXY signalling in turn regulates the WOX14, TMO6, LBD4 loop to
50 control vascular proliferation. Genetic interaction between *LBD4* and *PXY* suggests that
51 LBD4 marks the phloem-procambium boundary, thus defining the shape of the vascular
52 bundle. These data collectively support a mechanism that influences recruitment of cells into
53 the phloem lineage, and they define the role of PXY signalling in this context in determining
54 the arrangement of vascular tissue.

55 INTRODUCTION

56 In vascular plants, water is taken up from the soil but sugars are assimilated in leaves, so the
57 movement of these resources throughout the plant body is essential for plant survival. Xylem
58 and phloem are the specialized vascular tissues that perform this function. Both arise in a
59 highly ordered manner from meristematic divisions in the cambium and procambium.
60 Multiple mechanisms have been identified that influence vascular development (Fischer et
61 al., 2019); however, how these mechanisms interact to coordinate vascular morphogenesis is
62 poorly understood.

63

64 Auxin is central to vascular tissue specification, and its responses are mediated by, among
65 others, *MONOPTEROS* (*MP*), which encodes an Auxin Response Factor (ARF) (Hardtke and
66 Berleth, 1998). *Arabidopsis thaliana* (Arabidopsis) *mp* mutants are characterised by
67 patterning defects in the embryo vascular cylinder (Berleth and Jurgens, 1993). *MP* is thought
68 to act as an activator of vascular proliferation in seedlings (Vera-Sirera et al., 2015) or as a
69 repressor of vascular proliferation in mature plant tissues (Mattsson et al., 2003; Brackmann
70 et al., 2018). With additional signals, *MP* controls two pathways that stimulate vascular
71 proliferation. The first pathway is characterised by *TARGET OF MONOPTEROS5* (*TMO5*),
72 encoding a bHLH transcription factor (Schlereth et al., 2010) that with its homologues
73 promotes cell divisions in the vascular cylinder. These transcription factor genes are up-
74 regulated by *MP* in the embryo. *TMO5*-like proteins perform this function in heterodimers
75 with a second class of bHLH transcription factors including LONESOME HIGHWAY and its
76 relatives (Ohashi-Ito and Bergmann, 2007; De Rybel et al., 2013; De Rybel et al., 2014;
77 Ohashi-Ito et al., 2014; Vera-Sirera et al., 2015). The second pathway targeted by *MP*
78 comprises the auxin-responsive *TMO6* (Schlereth et al., 2010), which encodes a member of

79 the DOF family of transcription factors. Multiple members of the DOF family have been
80 shown to promote vascular cell divisions (Guo et al., 2009; Waki et al., 2013; Konishi et al.,
81 2015; Miyashima et al., 2019; Smet et al., 2019). The expression of a subset of *DOF* genes,
82 including *TMO6*, is also controlled by cytokinin (Miyashima et al., 2019). Thus, *TMO6*
83 responds to both cytokinin and auxin.

84

85 TRACHEARY ELEMENT DIFFERENTIATION INHIBITORY FACTOR (TDIF) and
86 PHLOEM INTERCALATED WITH XYLEM/TDIF RECEPTOR (PXY/TDR; referred to
87 hereafter as PXY) are a ligand-receptor pair (Hirakawa et al., 2008; Morita et al., 2016;
88 Zhang et al., 2016) that also promotes cell division in vascular meristems. The TDIF peptide
89 is derived from *CLE41*, *CLE42* and *CLE44*. These genes are expressed in the phloem while
90 *PXY* is expressed in the procambium (Ito et al., 2006; Fisher and Turner, 2007; Hirakawa et
91 al., 2008; Etchells and Turner, 2010). Upon TDIF binding to the PXY receptor, the
92 transcription factor genes *WOX4*, *WOX14*, and *ATHB8* are upregulated (Hirakawa et al.,
93 2010; Etchells et al., 2013). Another transcription factor, BES1, is also regulated by TDIF-
94 PXY. When TDIF binds to PXY, an interaction between PXY and GSK3 kinases results in
95 the phosphorylation and degradation of BES1. BES1 is thought to promote xylem
96 differentiation, so its degradation preserves cambium pluripotency (Kondo et al., 2014).

97

98 Interactions between TDIF-PXY and auxin signalling contribute to vascular tissue
99 development (Suer et al., 2011; Smetana et al., 2019). Both auxin and PXY responses are
100 mediated by interactions with GSK3 signalling proteins. GSK3s regulate the auxin response
101 via phosphorylation of ARFs, and during vascular development, this requires the absence of
102 active TDIF-PXY complexes (Cho et al., 2014; Kondo et al., 2014; Han et al., 2018). Auxin
103 also induces the expression of TDIF-PXY targets *ATHB8* and *WOX4* (Baima et al., 1995;
104 Mattsson et al., 2003; Suer et al., 2011). The induction of *TMO5-like1* (*T5L1*) and *LHW* also
105 increases *ATHB8* expression (Vera-Sirera et al., 2015). *ATHB8* encodes a HD-Zip III
106 transcription factor (Baima et al., 2001) whose paralogues modulate the expression of auxin
107 biosynthesis and auxin perception genes (Müller et al., 2016). HD-Zip III genes have wide-
108 ranging roles in vascular patterning and proliferation (Zhong and Ye, 1999; Emery et al.,
109 2003; Prigge et al., 2005; Carlsbecker et al., 2010; Baima et al., 2014; Ramachandran et al.,
110 2016).

111

112 In addition to PXY, a second family of receptor kinases, members of the ERECTA (ER)
113 family, control vascular expansion in Arabidopsis (Ragni et al., 2011; Uchida et al., 2012;
114 Uchida and Tasaka, 2013; Ikematsu et al., 2017). PXY and its paralogues genetically interact
115 with ER family members to control proliferation, cell size, and organisation in vascular
116 tissues (Etchells et al., 2013; Uchida and Tasaka, 2013; Wang et al., 2019). ER also interacts
117 with auxin signalling components and members of the HD-ZipIII family in developmental
118 contexts that include meristem maintenance, stem architecture, and leaf development
119 (Woodward et al., 2005; Chen et al., 2013). Thus, interactions between PXY, auxin,
120 cytokinin, HD-Zip IIIs, ER, and GSK3s constitute a significant proportion of the regulatory
121 mechanisms that define how vascular tissue develops.

122

123 How do these and other factors combine to coordinate vascular development at the level of
124 transcription? Here, to provide a framework for answering this question, we generated a
125 transcriptional regulatory network (TRN) incorporating a significant proportion of known
126 regulators of vascular development in Arabidopsis. We used high-throughput enhanced yeast-
127 one-hybrid (eY1H) assays (Gaudinier et al., 2011; Reece-Hoyes et al., 2011; Gaudinier et al.,
128 2017) to identify transcription factors that bind to the promoters of vascular regulators. Our
129 vascular development TRN comprises 690 transcription factor-promoter interactions. To
130 demonstrate the power of our network to identify novel regulators and interactions, we
131 characterised a feed-forward loop incorporating three transcription factors that link auxin and
132 PXY-mediated signalling: WOX14, TMO6, and LATERAL ORGAN BOUNDARIES
133 DOMAIN4 (LBD4). Feed-forward loops are often involved in dynamic gene regulation
134 (Mangan and Alon, 2003), and our results demonstrate that, in response to auxin and TDIF-
135 PXY signalling, the genes within this circuit define a zone of procambial activity to maintain
136 the arrangement of vascular tissue of the stem.

137

138 **RESULTS**

139 **Identification of putative TDIF target genes**

140 To generate a TRN downstream of TDIF, we first identified putative TDIF target genes. The
141 TDIF peptide ligand is derived from CLE41, CLE42 and CLE44 proteins, so we compared
142 the transcriptomes of mature (5-week-old) stem bases of *35S:CLE41* lines (i.e. increased
143 PXY signalling), to wild type. Genes were considered differentially expressed where the p-
144 value, adjusted for multiple hypothesis testing, was ≤ 0.05 (**Supplemental Data Set 1**).
145 *35S:CLE41* plants had on average 100.7 ± 9.1 undifferentiated cells per vascular bundle

146 compared to 59.5 ± 5.5 in the wild type (**Supplemental Figure 1A, B**). Consistent with the
147 vascular over-proliferation phenotype, genes shown to be predominantly expressed in the
148 procambium, including *BRI-LIKE1*, *PINFORMED1*, and *MP* (Gälweiler et al., 1998; Hardtke
149 and Berleth, 1998; Cano-Delgado et al., 2004), demonstrated significant increases in
150 expression in *35S:CLE41* plants relative to wild type (**Supplemental Table 1**). The
151 expression levels of previously described targets of PXY signalling, *ATHB8* and *WOX14*
152 (Hirakawa et al., 2010; Etchells et al., 2013), increased 2.78-fold ($p < 0.001$) and 4.76-fold,
153 respectively, in *35S:CLE41* vs. the wild type ($p < 0.001$). Our microarray data were further
154 validated using qRT-PCR of a select number of genes involved in xylem cell differentiation
155 or transcriptional regulation, including an *ASPARTIC PEPTIDASE* gene, *GMC*
156 *OXIDOREDUCTASE*, *MAP70-5*, *IAA30*, and *MYB38* (**Supplemental Figure 1**), and were
157 consequently used to guide promoter selection for eY1H experiments.

158

159 **A PXY-mediated transcriptional network for vascular development**

160 To understand how factors that control PXY-mediated vascular development interact, and to
161 identify novel vascular regulators, we identified transcription factor-promoter interactions
162 using enhanced Y1H assays (Gaudinier et al., 2011; Reece-Hoyes et al., 2011). Bait were
163 selected promoters from five groups of genes representing factors that regulate PXY-
164 mediated or xylem cell development in the inflorescence stem (**Supplemental Table 2**).
165 Group I included *PXY* and *PXL* receptors (Fisher and Turner, 2007), ligands (Ito et al., 2006),
166 and their target transcription factor gene, *WOX14* (Etchells et al., 2013). Group II comprised
167 *GSK3* family members, which interact with the PXY kinase domain (Kondo et al., 2014),
168 and their target transcription factor genes *BESI* and *BZRI* (He et al., 2002). The *ERECTA*
169 family (*ERf*) of receptors were included in group II, as ER-family receptors act in part
170 through *GSK3* signalling (Kim et al., 2012), and they genetically interact with PXY-family
171 receptors (Wang et al., 2019). Genes involved in auxin or cytokinin perception and auxin
172 responses that also demonstrated differential expression in *35S:CLE41* constituted groups III
173 and IV. These included *TMO6*, a transcriptional target of *MP* (Schlereth et al., 2010) and its
174 paralog *DOF1.8* (Le Hir and Bellini, 2013) (**Supplemental Table 2**). Promoters of *HD Zip-*
175 *III* transcription factor genes that were differentially expressed in *35S:CLE41* lines and have
176 been shown elsewhere to control vascular development (Zhong and Ye, 1999; Baima et al.,
177 2001; McConnell et al., 2001; Emery et al., 2003; Carlsbecker et al., 2010; Müller et al.,
178 2016) were used as bait for group V. Finally, based on very high expression in *35S:CLE41*,

179 *LBD4/ASL6* and its homologue, *LBD3/ASL9*, genes of unknown function were identified
180 (**Supplemental Table 2**).

181

182 We screened these promoters against a collection of 812 root-expressed transcription factors
183 that represent more than 95% of the transcription factors with enriched expression in the
184 Arabidopsis stele (Gaudinier et al., 2011; Taylor-Teeple et al., 2015). The resulting
185 interactions comprise a network consisting of 312 nodes (**Figure 1A**). Each node represents a
186 gene either as a promoter, as a transcription factor, or as both. The nodes were connected by
187 690 edges, each representing a transcription factor binding to a promoter, as identified in the
188 eY1H assays (**Figure 1A, Supplemental Data Set 2**). To visualize the nodes and edges, we
189 designed a custom layout in Cytoscape (Shannon et al., 2003). Promoter nodes were colored
190 and arranged in the five association groups described in the previous paragraph, i.e., PXY
191 signaling (group I; blue), ER/BRI1/GSK3 signaling (group II; mint), auxin/cytokinin
192 perception (group III green/red), targets of MP and affiliates (group IV orange/purple), and
193 HD-ZIP IIIs (group V, olive) (**Figure 1A**). Transcription factors are colored in white and
194 positioned in the network based on their target profile. Those targeting similar sets of
195 genes/groups were placed together. Transcription factors interacting with promoters in more
196 than two groups were placed at the center of the network. Those interacting with one or two
197 promoter groups were placed on the periphery. In total, 287 transcription factors targeted at
198 least one promoter in the network. The transcription factor families with the greatest
199 representation were AP2/EREBP transcription factors, of which 46 members interacted with
200 the screened promoters, followed by MYB (40 interactors), and C2H2 transcription factors
201 (31 interactors). A list of all interacting transcription factors and their respective classes is
202 shown in **Supplemental Data Set 3**.

203

204 We predicted that the network would be enriched for genes differentially expressed in
205 *35S:CLE41* (**Supplemental Figure 2A**). A significant enrichment ($p = 2.2e-6$) was observed
206 using a Fisher's exact test. Furthermore, using previously described loss-of-function gene
207 expression data from *p_{xy}* mutants (Etchells et al., 2012), a more dramatic enrichment ($p =$
208 $1.57e-62$; **Supplemental Figure 2B**) was observed. Thus, the network represents a PXY-
209 mediated transcriptional regulatory network.

210

211 **A WOX14-mediated feed-forward loop**

212 We used our predicted vascular development network (**Figure 1A**) combined with our
213 *35S:CLE41* transcriptome data (**Supplemental Data Set 1**) to identify a regulatory circuit for
214 further analysis. Promoters were ranked by the number of transcription factors that bound to
215 them (in-degree binding). *PHB*, *PHV*, *LBD4*, and *T5L1* demonstrated the highest levels of in-
216 degree connectivity in our TRN (**Supplemental Data Set 4**). In addition to its high in-degree
217 value of 68 (ranked 3rd), *LBD4* also demonstrated an 11-fold increase in expression in
218 *35S:CLE41* vs. the wild type (**Supplemental Table 1; Supplemental Data Set 1**), higher
219 than that of any other transcription factor. Furthermore, its function had not previously been
220 described, making it a strong candidate for further investigation.

221

222 *TMO6* and *WOX14* were predicted to bind to and regulate *LBD4* (**Figure 1B; Supplemental**
223 **Data Set 2**). Both were also expressed to a high degree in *35S:CLE41* lines, each
224 demonstrating a 4.8-fold increase in expression (**Supplemental Table 2, Supplemental Data**
225 **Set 1**). *WOX14* was also predicted to bind to and regulate both *TMO6* and *LBD4* (**Figure 1B;**
226 **Supplemental Data Set 2**); thus, these three transcription factors were present in a feed-
227 forward loop (**Figure 1B**). Feed-forward loops are enriched within xylem regulatory
228 networks (Taylor-Teeple et al., 2015) and ensure robust regulation of their target genes
229 (Shen-Orr et al., 2002; Mangan and Alon, 2003; Kalir et al., 2005; Kaplan et al., 2008). We
230 hypothesized that the *WOX14-TMO6-LBD4* feed-forward loop plays a key role in regulating
231 vascular development due to its potential to integrate auxin, cytokinin, and TDIF-PXY
232 signalling (**Figure 1A-B**). Specifically, *TMO6* is transcriptionally regulated by both auxin
233 (Schlereth et al., 2010) and cytokinin (Miyashima et al., 2019; Smet et al., 2019). *WOX14*
234 is regulated by TDIF-PXY (Etchells et al., 2013). Consequently, based on high network
235 connectivity and high expression in *35S:CLE41* relative to wild type, their likelihood of
236 integrating PXY, auxin, and cytokinin signalling, and their arrangement in a feed-forward
237 loop, we selected the regulatory circuit involving *TMO6*, *WOX14*, and *LBD4* for further
238 study.

239

240 **Genetic elimination of the *TMO6-WOX14-LBD4* feed-forward loop**

241 To determine the significance of the *TMO6-WOX14-LBD4* feed-forward loop in vascular
242 development, we genetically perturbed each of these genes singly and in combination. We
243 combined *wox14* (Etchells et al., 2013) and *lbd4* Arabidopsis T-DNA lines with *tmo6*
244 mutants generated by genome editing. The single mutants demonstrated no changes in the
245 number of cells per vascular bundle or vascular morphology compared to the wild type

246 (Figure 2A, F-G; Figure 3G, J-K; Supplemental Figure 3A-B, E-G; Etchells et al., 2013).
247 By contrast, the number of cells present per vascular bundle was significantly reduced in
248 *tmo6 wox14 lbd4* triple and *tmo6 wox14* double mutant stems ($p < 0.002$ and $p = 0.002$;
249 Figure 2A-F; Supplemental Data Set 5). Consistent with TMO6 and WOX14 acting as
250 upstream regulators of *LBD4*, as predicted from the eY1H data (Figure 1A), the *tmo6 wox14*
251 and *tmo6 wox14 lbd4* lines were indistinguishable ($p = 0.371$; Figure 2D, F).

252

253 In the wild type, vascular bundles expand to a greater degree along the radial axis of the stem
254 than the tangential, and thus vascular bundle shape can be measured by comparing
255 tangential:radial ratios. In the *tmo6 wox14 lbd4* lines, this ratio was higher than in wild type
256 (Figure 2G), and as such, the triple mutant demonstrated reduced expansion along the radial
257 axis of the stem. This genetic interaction supports the idea that the feed-forward loop
258 transcription factors are components of the same pathway and that they are critical for
259 controlling vascular proliferation and shape.

260

261 **WOX14 and TMO6 are sufficient to regulate gene expression within the feed-forward**
262 **loop in plant cells**

263 A prerequisite for *in planta* transcriptional regulation within the feed-forward loop is the
264 expression of *TMO6*, *WOX14*, and *LBD4* in the same place and time. Using *in situ*
265 hybridization, *TMO6* and *LBD4* mRNA antisense probes hybridised to cells in the vascular
266 tissue of the inflorescence stem, with expression maxima at the phloem-procambium
267 boundary (Figure 3A-B, Supplemental Figure 4A for sense controls). *WOX14:GUS*
268 expression (Figure 3C) was also present in phloem-procambium boundary cells, in addition
269 to other vascular cell types, and as described previously (Etchells et al., 2013).

270

271 Given the genetic interaction and overlapping expression of *TMO6*, *WOX14*, and *LBD4*, we
272 sought more direct evidence for the feed-forward loop interactions identified in eY1H *in*
273 *planta*. We transformed wild tobacco (*Nicotiana benthamiana*) leaf protoplasts with a
274 construct that harboured *LBD4pro:LUC* (*LUCIFERASE*) and *35S:REN* (*RENILLA*) cassettes
275 and determined *LBD4pro* activity as LUC activity normalised to that of REN. LUC activity
276 was higher in cells co-transformed with both *LBD4pro:LUC* reporter and a *35S:TMO6*
277 construct than in cells transformed with the *LBD4pro:LUC* reporter and a control (empty
278 vector) construct ($p < 0.001$; Supplemental Figure 5A). *LBD4* promoter activity further
279 increased ($p = 0.005$) when cells were co-transformed with *LBD4pro:LUC*, *35S:TMO6*, and

280 *35S:WOX14*. The LUC activity in cells containing both *LBD4pro:LUC* and *35S:WOX14* was
281 similar to that in cells harbouring *LBD4pro:LUC* and an empty vector control.

282

283 We used a similar strategy to verify WOX14-mediated regulation of transcripts under the
284 control of the *TMO6* promoter. Here, LUC activity was significantly higher ($p < 0.001$) when
285 *TMO6pro:LUC* was co-transformed with a *35S:WOX14* construct than when transformed
286 with a control construct (**Supplemental Figure 5B**). In summary, these multiple pieces of
287 data provide evidence that the WOX14-*TMO6*-*LBD4* transcription factor-promoter
288 interactions are sufficient to regulate transcription in plant cells (**Supplemental Figure 5**).

289

290 **Interconnected transcriptional regulation in the feed-forward loop**

291 We obtained *in planta* genetic evidence for these regulatory relationships by performing
292 qRT-PCR and examining loss-of-function mutant alleles. Our network suggested that *LBD4*
293 and *TMO6* act downstream of *WOX14* (**Figure 1B**), so we tested the expression levels of
294 these genes in *wox14* mutants in the basal third of 15 cm inflorescence stems, where *WOX14*
295 expression had previously been shown to be the highest. Because *WOX14* acts redundantly
296 with *WOX4* (Etchells et al., 2013), *wox4* and *wox4 wox14* lines were also included in our
297 analysis. Consistent with the notion that WOX14 regulates *TMO6* and *LBD4* expression,
298 *wox14* stems exhibited lower levels of *TMO6* and *LBD4* expression than wild type (**Figure**
299 **3D-E**). Thus, wild-type levels of *TMO6* and *LBD4* expression are dependent on the
300 expression of *WOX14*. Further reductions in *TMO6* and *LBD4* expression were not observed
301 in *wox4 wox14* lines relative to single *wox4* or *wox14* mutant alleles.

302

303 To determine if *LBD4* expression is also dependent on *TMO6* expression (**Figure 1B**), we
304 tested *tmo6* mutant lines. In the basal half of 15 cm inflorescence stems, *LBD4* expression
305 was unchanged in *tmo6* relative to wild type (**Figure 3F; Supplemental Table 3**). We
306 reasoned that the dependency of *LBD4* on *TMO6* might be revealed in a sensitised genetic
307 background. To test this hypothesis, we generated *wox4 wox14 tmo6* and *pxy pxl1 pxl2 tmo6*
308 (*pxf tmo6*) lines. *tmo6* dramatically enhanced the cell division defect observed in the *pxf*
309 triple mutants (**Figure 3G-J; Supplemental Data Set 5**), although the shapes of the bundles
310 (based on the tangential:radial ratio) did not differ from those of the *pxf* lines (**Figure 3K**).
311 We measured *LBD4* expression in the lower halves of inflorescence stems. The reductions in
312 *LBD4* expression in both the *pxf* and *wox4 wox14* lines proved not to be significant ($p = 0.167$
313 and $p = 0.102$; **Figure 3F; Supplemental Table 3**). By contrast, *LBD4* expression was

314 significantly lower in the *pxf tmo6* and *wox4 wox14 tmo6* mutants relative to wild type
315 ($p=0.031$ and $p=0.027$). Thus, while *LBD4* expression did not depend on the presence of
316 *TMO6* in the lower halves of 15 cm inflorescence stems, the reduced expression was
317 exacerbated in *tmo6 pxf* and *tmo6 wox4 wox14* relative to the parental lines (**Figure 3F**).
318 Therefore, *TMO6*, redundantly with TDIF/PXY signalling, regulates *LBD4* expression.

319

320 While these results supported the idea that *TMO6* and *WOX14* regulate *LBD4* expression,
321 they also raised the question of why *LBD4* expression was reduced in *wox4 wox14* lines when
322 the lower third of 15 cm inflorescence stems were sampled (**Figure 3E**), but not when the
323 lower half was sampled (**Figure 3F**). We reasoned that *LBD4* expression may vary along the
324 apical-basal axis of the stem and tested this hypothesis using qRT-PCR. *LBD4* expression
325 was significantly higher in the basal third of the inflorescence stem relative to the middle or
326 apical sections (**Supplemental Figure 4B**), which is consistent with the *LBD4* expression
327 levels observed in **Figures 3E and 3F**.

328

329 **TDIF-PXY dynamically regulates the feed-forward loop**

330 As *LBD4* expression was reduced in the *pxf tmo6* background, and *tmo6* genetically enhanced
331 the *pxf* phenotype (**Figure 3I-K**), we further explored the expression of genes in this feed-
332 forward loop in response to perturbations in TDIF-PXY signalling. We measured *LBD4* and
333 *TMO6* expression in *pxf* (Fisher and Turner, 2007; Wang et al., 2019) and in *cle41 cle42*
334 *cle43 cle44* mutants (referred to hereafter as *tdif*; **Supplemental Figure 6**), which were
335 generated by genome editing. Here, specifically, we measured gene expression in the lower
336 third of 10 cm stems. A significant reduction in *LBD4* expression was not observed, but
337 reduced *TMO6* expression was observed (**Figure 4A,B**). These results demonstrate that
338 *TMO6* is responsive to genetic perturbation of TDIF-PXY signalling.

339

340 To determine the temporal dynamics of gene regulation within the feed-forward loop, we
341 applied TDIF or control peptide to five-day-old wild type, *pxy*, and *wox4 wox14* seedlings.
342 *WOX14* expression increases upon TDIF application (Etchells et al., 2013). Similarly, a 2-
343 hour treatment with 5 μ M TDIF in wild-type plants resulted in increased *LBD4* and *TMO6*
344 expression relative to plants treated with a P9A negative control (**Figure 4C,D**). This
345 induction of *TMO6* and *LBD4* was absent, and their expression even further reduced, in *pxy*
346 and *wox4 wox14* mutants, suggesting that PXY/TDIF activate the expression of all genes
347 within the feed-forward loop (**Figure 4A-D**).

348

349 **The WOX14-TMO6-LBD4 feed-forward loop is auxin responsive**

350 MP is a transcriptional regulator of *TMO6* (Schlereth et al., 2010), and crosstalk between
351 auxin and TDIF-PXY signalling has been described (Suer et al., 2011; Han et al., 2018). We
352 therefore tested the expression of all three transcription factors in the feed-forward loop upon
353 exposure to 10 μ M IAA. *TMO6* and *LBD4* expression increased in response to a 6-hour auxin
354 treatment in both wild type and *wox14* mutants, demonstrating that auxin regulates *LBD4* and
355 *TMO6* expression in a *WOX14*-independent manner (**Figure 4E-F**). *WOX14* was also
356 upregulated in response to auxin treatment (**Figure 4G**).

357

358 ***LBD4* regulates vascular cell number and organization**

359 To determine the function of this feed-forward loop in vascular development, we
360 characterized vascular development in inflorescence stems upon genetic perturbation of the
361 final gene within the feed-forward loop, *LBD4*. The phenotype of the *lbd4* single mutant was
362 similar to that of the wild-type controls (**Figure 2F-G; Supplemental Figure 3A-B;**
363 **Supplemental Data Set 5**). To eliminate functional redundancy, we crossed *lbd4* to a T-
364 DNA insertion line of *LBD3*, the gene most similar to *LBD4* (Shuai et al., 2002). A reduction
365 in vascular cell number was observed in *lbd3 lbd4* double mutants (**Supplemental Figure**
366 **3D-E**).

367

368 *LBD4* is expressed at the procambium-phloem boundary (**Figure 3A**). Thus, we determined
369 phloem cell number in the *lbd3 lbd4* double mutants and controls, but no differences were
370 observed (**Supplemental Figure 3E; Supplemental Data Set 5**). We also measured the
371 distribution of phloem along the radial axis in these lines. The *lbd3 lbd4* double mutants had
372 a thinner band of phloem in vascular bundles than the control lines (**Supplemental Figure**
373 **3F**), although this did not influence overall vascular bundle shape, as judged by measuring
374 the tangential:radial ratio (**Supplemental Figure 3G**). Other members of the *LBD* gene
375 family define boundaries at the edges of the apical meristem and the lateral root (Okushima et
376 al., 2007; Bell et al., 2012). *LBD4* is expressed at the phloem-procambium boundary and
377 influences phloem distribution redundantly with *LBD3*. Thus, we reasoned that *LBD4* might
378 influence boundaries within vascular tissue. To explore this idea, we manipulated the *LBD4*
379 expression domain. *LBD4* expression was restored ectopically in companion cells of the
380 phloem using a *SUC2:LBD4* construct or in the xylem using an *IRX3:LBD4* construct, both
381 within the *lbd4* mutant background (**Figure 5**). In *lbd4 SUC2:LBD4* lines, an increase in the

382 total number of cells per vascular bundle was observed. While xylem cell number did not
383 differ between genotypes, both phloem and procambium cell numbers were higher in *lbd4*
384 *SUC2:LBD4* than in the other lines (**Figure 5D**).

385

386 We observed reduced secondary cell wall deposition in the fiber cells of *lbd4 IRX3:LBD4*
387 lines (**Figure 5A,C**), indicating that xylem differentiation was disrupted, although the total
388 number of cells in the xylem did not change (**Figure 5D**). In terms of overall vascular bundle
389 shape within these different backgrounds, the ratio of the length of the tangential to radial
390 axes of vascular bundles was 0.65 in wild type, which is similar to that observed in *lbd4* and
391 *lbd4 SUC2:LBD4* lines (**Figure 5E**). By contrast, the ratio increased to 0.96 in *lbd4*
392 *IRX3:LBD4* vascular bundles, demonstrating a reduction in vascular expansion along the
393 radial axis relative to the tangential axis. Furthermore, phloem distribution was dramatically
394 different in the *LBD4* misexpression lines. The *lbd4 SUC2:LBD4* lines exhibited a wider
395 band of phloem along the radial axis compared to the other lines tested (**Figure 5E**). While
396 this can be explained in part by changes to phloem cell number, the same cannot be said of
397 changes to phloem distribution in *lbd4 IRX3:LBD4* lines. Here, despite similar numbers of
398 phloem cells relative to wild type or *lbd4* single mutants (**Figure 5D**), these phloem cells
399 were distributed in a much narrower band (**Figure 5E**). The redistribution of phloem cells
400 accompanied by changes to vascular bundle shape could be caused by a failure to correctly
401 mark the phloem-procambium boundary.

402

403 **The vascular function of LBD4 is PXY/TDIF-dependent**

404 *pxy* and *tdif* mutants demonstrate intercalation of vascular cell types, i.e., a loss of clearly
405 defined boundaries (**Figure 6, Supplemental Figure 6**)(Fisher and Turner, 2007; Etchells
406 and Turner, 2010; Wang et al., 2018). These mutants are also characterised by reductions in
407 vascular cell number (Hirakawa et al., 2008). To investigate genetic interactions between *pxy*
408 and *lbd4*, we generated *pxy lbd4* double mutants. The gross morphology of these plants did
409 not differ from that of the *pxy* single mutants, but *lbd4* enhanced the cell division phenotype
410 of *pxy*, as *pxy lbd4* bundles had fewer cells per vascular bundle than the parental lines
411 (**Figure 6A; Supplemental Data Set 5**). We counted the number of differentiated phloem
412 cells to assess the recruitment of phloem precursors into the phloem. These numbers were
413 similar in *pxy lbd4* lines compared to *pxy* and *lbd4* single mutants but were reduced compared
414 to wild type (**Figure 6B; Supplemental Data Set 5**). *lbd4* also enhanced the defect in
415 phloem distribution along the vascular radial axis of *pxy* (**Figure 6C; red arrowheads in**

416 **6E**). Finally, the tangential:radial axis ratio of vascular bundles was higher in the *lbd4 pxy*
417 lines relative to the controls (**Figure 6D**), demonstrating a change to overall vascular bundle
418 shape.

419

420 Vascular organisation requires that *CLE41/42/44* generate a TDIF maximum in the phloem.
421 Ectopic *CLE41* expression leads to intercalated xylem and phloem, presumably due to a
422 change in the distribution of active TDIF-PXY complexes (Etchells and Turner, 2010). *LBD4*
423 expression is elevated in response to TDIF-PXY (**Figure 4C; Supplemental Table 1**). Thus,
424 we predicted that the defects of *IRX3:CLE41* would be attenuated in the absence of *LBD4*.
425 Cell number within vascular bundles was unchanged in *lbd4* but significantly increased in
426 *IRX3:CLE41* compared to the wild type (**Figure 6F,G**). Introduction of the *lbd4* mutation
427 into *IRX3:CLE41* lines suppressed this phenotype. The tangential:radial ratio of *IRX3:CLE41*
428 *lbd4* lines was indistinguishable from that of wild type and *lbd4* (**Figure 6H**). Thus, the
429 changes to vascular bundle shape caused by the *IRX3:CLE41* construct were dependent on
430 *LBD4*. Intercalation of xylem and phloem was also reduced in *IRX3:CLE41 lbd4* compared to
431 *IRX3:CLE41*. Finally, *lbd4* attenuated the gross morphological defects of *IRX3:CLE41*
432 (**Supplemental Figure 7**). Thus, *lbd4* suppresses the *IRX3:CLE41* phenotype.

433

434 **DISCUSSION**

435 **Integration of transcriptional regulators of vascular development**

436 The study of vascular tissue development in plants has a long history. In addition to
437 characterisation by early plant anatomists, auxin in particular was found to influence vascular
438 formation and connectivity in the 1950s and 60s (Torrey, 1953; Sun, 1955; Sachs, 1969). In
439 the 1990s, with the emergence of Arabidopsis as a genetic model, multiple genes were
440 characterised as regulating vascular tissue formation (Lincoln et al., 1990; Berleth and
441 Jurgens, 1993; Baima et al., 1995; Zhong et al., 1997; Gälweiler et al., 1998), and such
442 discoveries have been accelerating in the post-genomic era (Ruonala et al., 2017; Fischer et
443 al., 2019). Recently, those taking genetic, biochemical, and mathematical approaches to
444 studying vascular development have elegantly described how a subset of these components
445 interact (De Rybel et al., 2014; Kondo et al., 2014; Muraro et al., 2014; Vera-Sirera et al.,
446 2015; Mellor et al., 2016; Han et al., 2018; Miyashima et al., 2019; Smet et al., 2019). Here,
447 we used an enhanced Y1H approach to map a network with 312 nodes and 690 interactions
448 that describes how numerous components may come together to control the patterning and
449 proliferation of vascular tissue (**Figure 1A**). Because we screened the promoters of

450 components involved in auxin perception, cytokinin perception, PXY receptors, ER
451 receptors, and GSK3 kinases, the network can be used to identify transcription factors that
452 integrate these signals. This set of transcription factor-promoter interactions represents PXY-
453 mediated transcriptional regulation, as perturbations in the TDIF-PXY signalling pathway
454 (genes differentially expressed in *pxy* mutants and in *35S:CLE41* lines) are significantly
455 enriched within our network (**Supplemental Figure 2**).

456

457 **The TMO6-WOX14-LBD4 feed-forward loop is essential for vascular development**

458 The power of our network as a resource for identifying novel interactions was demonstrated
459 by characterizing the TMO6-WOX14-LBD4 feed-forward loop. We investigated the nature
460 of this regulatory circuit using eY1H, LUC reporter assays, qRT-PCR, and genetic interaction
461 analysis. The regulatory circuit appears to be central to vascular cell proliferation, as
462 evidenced by the loss of 41% of vascular bundle cells in *tmo6 wox14 lbd4* lines relative to
463 wild type (**Figure 2F**). We demonstrated that the feed-forward loop is regulated by auxin and
464 TDIF-PXY signalling (**Figures 3F-K; 4A-D; 6; Supplemental Table 1**)(Etchells et al.,
465 2013). Given that TMO6 has also been shown to be an integrator of cytokinin signalling
466 (Schlereth et al., 2010; Miyashima et al., 2019; Smet et al., 2019), this circuit likely acts as an
467 integration point for many critical developmental regulators.

468

469 The transcription of *HD-ZIP III* genes is thought to be activated by the TMO6 paralogue
470 PEAR1 during primary patterning of the root vascular cylinder (Miyashima et al., 2019). In
471 our eY1H assays, both PEAR1 and TMO6 bound to the promoters of *HD-ZIP III* genes *PHB*,
472 *PHV*, and *REV* (**Figure 1A; Supplemental Data Set 2**). *HD-ZIP III* expression is thought to
473 represses *PEAR1* transcription in a negative feedback loop (Miyashima et al., 2019), and
474 *PHV* bound the *TMO6* promoter in our eY1H assay (**Figure 1A; Supplemental Data Set 2**).
475 Therefore, it would be interesting to further study interactions between *HD-ZIP III* genes,
476 *PEAR1*, and members of the feed-forward loop.

477

478 **Members of the feed-forward loop may function redundantly with paralogues**

479 Genetic redundancy, such as that uncovered by Miyashima et al. (2019), is a possible
480 explanation for the finding that the *tmo6* mutants demonstrated no changes in *LBD4*
481 expression (**Figure 3F**). Genetic redundancy might also explain the lack of mutant
482 phenotypes for individual *LBD* family members. A recent genetic analysis aimed at
483 characterising regulators of the vascular cambium in Arabidopsis roots also identified *LBD4*

484 as a putative vascular regulator (Zhang et al., 2019). *lbd1 lbd4* lines exhibited reduced
485 vascular tissue area in roots. Since we demonstrated that *lbd4* acts redundantly with *lbd3*
486 (**Supplemental Figure 3**), it is tempting to speculate that there may be genetic redundancy
487 between these three paralogues.

488

489 **Control of vascular bundle size and shape**

490 *TMO6*, *WOX14*, and *LBD4* are jointly expressed at the phloem-procambium boundary in the
491 vascular tissue of inflorescence stems (**Figure 3A-C**). These genes also act within a coherent
492 type I feed-forward loop (Mangan and Alon, 2003), as all are positive transcriptional
493 activators. *WOX14* was sufficient to activate *TMO6* expression in wild tobacco protoplasts
494 (**Supplemental Figure 5**) and was also required for normal expression of *TMO6* in
495 Arabidopsis stems (**Figure 3D**). *WOX14* activated *LBD4* reporter expression in wild tobacco
496 protoplasts when co-expressed with *TMO6* (**Supplemental Figure 5A**). Both *WOX14* and
497 *TMO6* were required for the very highest levels of *LBD4* expression in wild tobacco
498 (**Supplemental Figure 5A**). Such synergism may also explain why *tmo6* mutants alone did
499 not demonstrate changes to *LBD4* expression, but *pxf tmo6* (where *WOX14* expression is
500 reduced) and *wox4 wox14 tmo6* lines did (**Figure 3F**).

501

502 *WOX* genes and their targets are crucial for regulating stem cell fate in plant meristems (Laux
503 et al., 1996; Sarkar et al., 2007; Ji et al., 2010; Etchells et al., 2013), but the roles of direct
504 *WOX* targets in the vascular stem cell niche have been unclear. Modelling of transcriptome
505 data in Zhang et al. (2019) also placed *WOX14* upstream of *LBD4*. The data presented here
506 provide additional support for this interaction (**Figures 1B, 3D-F, Supplemental Figure 5**).

507

508 **Organ boundaries are marked by members of the *LBD* family**

509 Members of the *LBD/AS2* gene family (Iwakawa et al., 2002; Shuai et al., 2002) regulate the
510 formation of organ boundaries during lateral root formation (Okushima et al., 2007) and at
511 the shoot apex (Bell et al., 2012) in Arabidopsis. In hybrid poplar (*Populus tremula* ×
512 *Populus alba*), the overexpression of *PtaLBD1* increases secondary phloem production
513 (Yordanov et al., 2010). Here, we determined that *LBD4* is expressed at the phloem-
514 procambium boundary (**Figure 3A**). An increase in vascular bundle cell number was
515 observed in *lbd4 SUC2:LBD4* lines, where *LBD4* expression was shifted to the phloem.
516 Increases in cell number were restricted to the procambium and phloem. Strikingly, no
517 change in the number of xylem cells was observed (**Figure 5D**). These data suggest that

518 *LBD4* controls phloem cell recruitment in a spatially restricted manner (**Figure 5A,B,E**). The
519 loss of normal xylem differentiation in *lbd4 IRX3:LBD4* bundles where *LBD4* expression was
520 shifted to the xylem (**Figure 5C**) suggests that this occurs in part by excluding xylem identity
521 from the phloem side of the procambium. *LBD4* could mark the phloem-procambium
522 boundary via regulation by TDIF-PXY, WOX14, and TMO6. Notably, *TMO6* and its
523 paralogues are thought to define the zone of procambial activity in the root (Miyashima et al.,
524 2019). The definition of the procambium domain could be considered to include marking its
525 edges. Thus, *LBD4* could act as a boundary regulator or as an amplifier of divisions on the
526 phloem side of the procambium. These putative functions are not necessarily mutually
527 exclusive.

528

529 **TDIF-PXY and LBD4**

530 *pxy* mutants are characterised by intercalation of xylem and phloem (Fisher and Turner,
531 2007). For such phenotypes to occur, boundary specification must be disrupted. In *pxy lbd4*
532 mutants, the positions of tissues were altered because phloem was distributed differently
533 along the radial axis of the stem (**Figure 6C**) and bundle shape was altered (**Figure 6D**). *lbd4*
534 *pxy* plants also demonstrated reductions in vascular cell division (**Figure 6A-B**). PXY-
535 regulated vascular organisation is dependent on *CLE41* acting as a phloem-derived positional
536 cue. Dramatic vascular reorganisation occurs when *CLE41* is expressed from the xylem in
537 *IRX3:CLE41* lines because the position of active TDIF-PXY complexes is altered (Etchells
538 and Turner, 2010). In turn, this leads to changes in the positions of xylem, phloem, and
539 procambium (**Figure 6F**) and as such, these tissues are found in ectopic positions relative to
540 wild type. Consequently, boundaries between the phloem and procambium must also be
541 present in ectopic positions in *IRX3:CLE41*. Our observation that the *IRX3:CLE41* phenotype
542 was strongly suppressed by *lbd4* supports the hypothesis that *LBD4* marks the phloem-
543 procambium boundary, since in *lbd4 IRX3:CLE41* plants, phloem was restored to the position
544 it occupied in the wild type (**Figure 6F**). Therefore, the putative ectopic *LBD4*-specified
545 boundary tissue observed in *IRX3:CLE41* lines was removed in these plants.

546

547 In conclusion, a genetic interaction between *LBD4* and *PXY* regulates vascular bundle shape.
548 *LBD4* also determines stem cell number in the vascular meristem via regulation by *TMO6*
549 and *WOX14* and redundantly with *LBD3*. Our PXY-mediated transcriptional network
550 provides a framework for exploring other interacting regulators at the transcriptional level.

551 **METHODS**

552 **Gene expression analysis**

553 Microarray analysis was used to compare the transcriptomes of *Arabidopsis thaliana* Col-0
554 and *35S:CLE41*; the experimental set up, preparation of total RNA, synthesis of biotinylated
555 cDNA, subsequent hybridization to ATH1 Affymetrix GeneChip oligonucleotide arrays, and
556 detection were described previously (Etchells et al., 2012). Briefly, following germination on
557 MS agar plates, plants were transferred to soil and grown under long-day conditions (see
558 below) for 5 weeks. Inflorescence stems were harvested, stripped of side branches, and
559 divided into four sections of equal size. RNA was isolated from the third section from the top
560 using TRIzol (Invitrogen). Samples were prepared in triplicate for each genotype, and
561 following RNA extraction, processing was carried out at the University of Manchester
562 Genomic Technologies Facility
563 (<http://www.ls.manchester.ac.uk/research/facilities/microarray/>). Technical QC was
564 performed as described (Li and Wong, 2001), and background correction, normalization, and
565 gene expression analysis were performed using RMA in Bioconductor (Bolstad et al., 2003).
566 Differential expression analysis was performed using Limma (Smyth, 2004). No probe is
567 present for the *WOX4* gene on this microarray chip.

568

569 Gene expression in inflorescence stems was compared by quantitative RT-PCR using RNA
570 isolated with TRIzol reagent (Life Technologies). Samples were measured in technical
571 triplicates (reactions per sample) on biological triplicates (independent samples per genotype
572 and/or treatment). The RNA was DNase treated with RQ1 (Promega) prior to cDNA
573 synthesis using a poly-T primer and BioScript reverse transcriptase (Bioline). qPCR BIO
574 SyGreen Mix (PCR Biosystems) and primers described in **Supplemental Data Set 6** were
575 used with a CFX Connect machine (BioRad). Relative expression was determined using a
576 comparative threshold cycle (Ct) method using average amplification efficiency for each
577 primer pair, as determined using LinReg (Ramakers et al., 2003). Samples were normalised
578 to 18S rRNA (not shown) and *ACT2* (shown). Results were similar regardless of the control
579 used.

580

581 To characterize changes in gene expression in response to TDIF and P9A peptides, or IAA
582 application, seeds were stratified prior to incubation in a Sanyo MLR-351H plant growth
583 chamber set to 23°C and constant light on ½× MS with 1% agar. At 5 days, seedlings were
584 transferred to liquid ½ × MS medium containing either 5 µM TDIF (His-Glu-Val-Hyp-Ser-
585 Gly-Hyp-Asn-Pro-Ile-Ser-Asn) or negative control P9A (His-Glu-Val-Hyp-Ser-Gly-Hyp-

586 Asn-Ala-Ile-Ser-Asn; Bachem, Switzerland), or 10 μ M IAA. Plants were maintained on a
587 rocking platform for 1 hour, snap frozen in liquid nitrogen, and subjected to RNA extraction
588 and qRT-PCR analysis as described above.

589

590 **eY1H assays**

591 Yeast cells were grown using standard methods (Brady et al., 2011; Gaudinier et al., 2011;
592 Reece-Hoyes et al., 2011; Taylor-Teeple et al., 2015). Briefly, YPDA medium was used for
593 unrestrained growth. -Trp, -His-Ura, or -His-Ura-Trp (containing 3AT when necessary)
594 medium was used apply selection. The transcription factor library contained 812 unique
595 cDNAs fused to the GAL4 activation domain in pDEST-AD-2 μ , which are maintained as
596 plasmids in yeast and enable growth on -Trp medium. For promoter clones, promoter
597 fragments (1.2-3.5 kb) were amplified using LA taq (Takara) and cloned using 5'TOPO (Life
598 Technologies). These entry clones were used to create reporter constructs via Gateway
599 recombination. The use of pMW2 clones enabled selection on -His medium and detection of
600 interactions via growth on plates supplemented with 3AT. pMW3 (selection on -Ura
601 medium) contained a LacZ reporter. Both vectors were transformed into yeast strain
602 YM4271, integrated into the yeast genome via homologous recombination, and selected on -
603 His -Ura plates. Colonies with no autoactivation in X-gal that grew on moderate 3AT
604 concentrations (10-100 mM) were selected. The presence of both reporters was confirmed by
605 PCR.

606

607 eY1H was performed as described (Gaudinier et al., 2011; Reece-Hoyes et al., 2011) using a
608 RotoR HD robot (Singer). Briefly, mating was carried out by combining yeast cells
609 containing the transcription factor and promoter constructs on a YPDA plate. After diploid
610 selection using -His -Ura -Trp plates, the diploids were plated onto plates supplemented with
611 3AT, and onto YPDA plates containing a nitrocellulose filter. Following two days of growth
612 at room temperature, the nitrocellulose filters were subjected to an X-gal assay. For 3AT
613 plates, the plates were checked daily for colonies with increased growth. A network was
614 subsequently constructed by importing the directional interactions into Cytoscape.

615

616 **Testing transcription factor-promoter interactions**

617 To test transcription factor-promoter interactions using a dual luciferase assay system, target
618 promoters were cloned upstream of the *LUC* reporter gene in pGreenII-0800-LUC, which
619 also contained a *35S:REN* control cassette. Transcription factor sequences were cloned

620 behind the 35S promoter in pGreenII 62-SK (Hellens et al., 2005). A ClonExpress II One
621 Step Cloning Kit (Vazyme), and primers listed in **Supplemental Data Set 6** was used for
622 vector construction. Reporter detection was performed using the Dual-Luciferase Reporter
623 Assay System (Promega). Boxplots in **Supplemental Figure 5** show data from four
624 biological replicates.

625

626 Wild tobacco leaf protoplasts were generated by immersing leaf material in a solution
627 containing 1.5% CellulaseR10 (Yakult), 0.2–0.4% MacerozymeR10 (Yakult), 1%
628 HemiCellulase (sigma), 0.4 M mannitol, 20 mM KCl, 20 mM MES (pH 5.7), 10 mM CaCl₂,
629 0.1% BSA for 12 h. An equal volume of W5 solution (150 mM NaCl, 125 mM CaCl₂, 5 mM
630 KCl, 2 mM MES [pH 5.7]) was added prior to passing the mixture through a 200-mesh sieve.
631 Protoplasts were collected by centrifugation and resuspended in ice-cold W5 (Duarte et al.,
632 2016). Purified plasmids were transferred into these cells using the PEG–calcium method
633 with minor modifications (Yoo et al., 2007).

634

635 **Generation of plant stocks**

636 Seeds were stratified for 2 d at 4°C in 0.1% agar prior to sowing on a mix of 75% Levington
637 F2 compost or on Murashige and Skoog (MS) medium, 1% agar (w/v) on vertical plates.
638 Plants were grown at 22°C under long-day conditions (16 h light/8 h dark, 300 μmol m⁻²
639 s⁻¹, provided by cool-white fluorescent bulbs, supplemented with incandescent lighting).

640 Seed lines were all in the Col-0 background. 35S:*CLE41*, *pxy-3*, *wox4*, *wox14*, *IRX3:CLE41*,
641 *IRX3:CLE41 wox4*, *pxf* (*pxy pxl1 pxl2*) have been described previously (Fisher and Turner,
642 2007; Etchells and Turner, 2010; Hirakawa et al., 2010; Etchells et al., 2013)(**Supplemental**
643 **Table 4**). *lbd3* (WiscDsLoxHs070_10G) (Woody et al., 2007) and *lbd4* (Salk_146141)
644 (Alonso et al., 2003) mutant lines (**Supplemental Table 4**) were identified using the TAIR
645 database (Swarbreck et al., 2008) and confirmed using PCR. The *lbd4* allele harboured the T-
646 DNA insertion in the *LBD4* 5' UTR, and we could not detect *LBD4* mRNA using qRT-PCR.
647 *pxy lbd4*, *lbd3 lbd4*, *wox4 lbd4* and *IRX3:CLE41 lbd4* lines were identified in segregating F2
648 populations by PCR. *tmo6* lines (**Supplemental Table 4**) were generated by genome editing
649 (Xing et al., 2014; Wang et al., 2015). Target sequences AAGAAACCTTCTCCTGCAA and
650 CTCTAAGGAACATCCCCGTG were identified using CRISPR-PLANT (Xie et al., 2014)
651 and tested for off-targets (Bae et al., 2014). Primers incorporating the target sequences
652 (**Supplemental Data Set 6** were used in a PCR with plasmid pCBC-DT1T2 as template to
653 generate a PCR product with a *TMO6* guide RNA, which was in turn incorporated into

654 pHEE2E-TRI using a Golden Gate reaction. The resulting *TMO6* CRISPR/Cas9 clone was
655 transferred to Arabidopsis by the floral dip method (Clough and Bent, 1998). Mutants were
656 selected with primers that flanked the guide RNA target sites (**Supplemental Figure 8**).
657 Oligonucleotides used for genotyping are described in **Supplemental Data Set 6**.

658

659 The CRISPR construct used to generate the *cle41,42,43,44* (*tdif*) mutant was built using the
660 *pCUT* vector system (Peterson et al., 2016). For each of the four targeted CLE genes, a 20 bp
661 gRNA target site was selected upstream of the dodecapeptide coding region in the genomic
662 sequence. A gRNA gene array was synthesized by GeneArt (Thermo Fisher) as a group of
663 four *AtU6:gRNA* tandem constructs, which was subsequently cloned into the *pCUT4* binary
664 vector via restriction enzyme digestion methods as previously described (Peterson et al.,
665 2016). Col-0 plants were transformed with the CRISPR binary construct via the floral dip
666 method and T1 transgenic seed derived was selected on B5 medium without sucrose and
667 containing 100 mg/L hygromycin. The T1 generation was screened for editing efficiency by
668 sequencing the CLE gene PCR products amplified from leaf DNA. Plants confirmed to have
669 efficient editing had overlapping sequence traces originating at the -3 position from the PAM.
670 T2 seed derived from plants with efficient editing was grown on selective B5 medium, DNA
671 was collected, and each of the four *CLE* target genes was amplified via PCR. The products
672 were sequenced directly via Sanger sequencing using primers listed in Supplemental Data Set
673 6. These plants demonstrated a *pxy*-like phenotype, which was partially recoverable by
674 transformation with a *SUC2:CLE41* construct (**Supplemental Figure 6**) that was described
675 previously (Etchells and Turner, 2010).

676

677 The *wox14 lbd4 tmo6* lines and respective double mutants were identified in F2 and F3
678 populations. *IRX3:LBD4* and *SUC2:LBD4* lines were generated by PCR amplification of a
679 genomic fragment incorporating the *LBD4* coding region, which was cloned into pENTR-D-
680 TOPO prior to transfer into plasmid p3KC (Atanassov et al., 2009). For *SUC2:LBD4*, the
681 *IRX3* promoter in p3KC was replaced with that of *SUC2*. The resulting over-expression
682 clone was introduced into Arabidopsis using the floral dip method (Clough and Bent, 1998).

683

684 **Histology**

685 Plant vascular tissue visualisation was carried out in 4 µm resin sections stained with 0.05%
686 aqueous toluidine blue, following fixation of plant material in FAA, dehydration through an
687 ethanol series, and embedding in JB4 resin. Alternatively, hand sections were stained with

688 500 mM aniline blue dissolved in 100 mM phosphate buffer, pH 7.2 and viewed under a UV
689 lamp.

690

691 **Accession numbers**

692 The accession numbers of the factors central to this paper are CLE41 (AT3G24770), CLE42
693 (AT2G34925), CLE44 (AT4G13195), LBD3 (AT1G16530), LBD4 (AT1G31320), PXL1
694 (AT1G08590), PXL2 (AT4G28650), PXY (AT5G61480), TMO6 (AT5G60200), WOX4
695 (AT1G46480), and WOX14 (AT1G20700). For a comprehensive list of accession numbers
696 represented in the eY1H data, please see **Supplemental Data Set 2**.

697 Microarray data have been submitted in a MIAME compliant standard to GEO (accession
698 number GSE123162).

699

700 **Supplemental Data**

701 **Supplemental Figure 1.** qRT-PCR confirmation of microarray experiment.

702 **Supplemental Figure 2.** Network of genes misexpressed in different genetic backgrounds.

703 **Supplemental Figure 3.** Vascular tissue in *lbd3 lbd4* double mutants.

704 **Supplemental Figure 4.** *In situ* controls, and *LBD4* expression along the apical-basal axis of
705 wild type and *pxy* mutant stems

706 **Supplemental Figure 5.** *LBD4pro:LUC* expression in the presence of WOX14 and TMO6.

707 **Supplemental Figure 6.** Phenotype of *cle41 cle42 cle43 cle44* quadruple mutants.

708 **Supplemental Figure 7.** *lbd4* suppresses the *IRX3:CLE41* phenotype.

709 **Supplemental Figure 8.** Genome edited *tmo6* allele.

710 **Supplemental Table 1.** Expression of genes demonstrating expression changes in
711 35S:CLE41 compared to wild type in array data analysed in this study.

712 **Supplemental Table 2.** Promoters analysed using Y1H.

713 **Supplemental Table 3.** P-values for qRT-PCR analysis of *LBD4* expression differences in
714 *pxf tmo6* and *wox4 wox14 tmo6* mutants and controls.

715 **Supplemental Table 4.** Plant lines used in this manuscript.

716 **Supplemental Data Set 1.** Differentially expressed genes in 35S:CLE41 compared to wild
717 type, as determined using microarrays.

718 **Supplemental Data Set 2.** Transcription factor-promoter interactions identified in eY1H.

719 **Supplemental Data Set 3.** List of interacting transcription factors and the transcription
720 factors families that they represent.

721 **Supplemental Data Set 4.** Promoters arranged in order of those with the most to fewest
722 interacting transcription factors.

723 **Supplemental Data Set 5.** Pairwise p-values for all comparisons of vascular phenotypes in
724 this manuscript.

725 **Supplemental Data Set 6.** Oligonucleotides used in this study.

726

727 **ACKNOWLEDGEMENTS**

728 The authors gratefully acknowledge financial support from via a Marie Skłodowska-Curie
729 fellowship to JPE, N8 Agrifood pump priming finds to JPE and SRT, the Jo Kolk Study Fund
730 from the VVAO to MES. This research was supported by a National Science Foundation
731 Plant Genome Research Program (IOS-1546837) to ZLN. SMB was partially funded through
732 a Howard Hughes Faculty Scholar fellowship. We thank Dória de Souza-Etchells for
733 technical assistance.

734

735 **AUTHOR CONTRIBUTIONS**

736 S.M.B., J.P.E., S.R.T., D.W., J.T.K., X.Y., H.S., Z.L.N. designed the experiments. M.E.S.,
737 S.M., H.S., C.G., A.M.B., C.L.S., A.G., C.J.W., J.T.K., and J.P.E. performed the
738 experiments. All authors analysed the data. J.P.E. and S.M.B. drafted the manuscript.

739

740 **REFERENCES**

741 **Alonso, J.M., Stepanova, A.N., Leisse, T.J., Kim, C.J., Chen, H., Shinn, P., Stevenson,**
742 **D.K., Zimmerman, J., Barajas, P., Cheuk, R., Gadrinab, C., Heller, C., Jeske, A.,**
743 **Koesema, E., Meyers, C.C., Parker, H., Prednis, L., Ansari, Y., Choy, N., Deen,**
744 **H., Geralt, M., Hazari, N., Hom, E., Karnes, M., Mulholland, C., Ndubaku, R.,**
745 **Schmidt, I., Guzman, P., Aguilar-Henonin, L., Schmid, M., Weigel, D., Carter,**
746 **D.E., Marchand, T., Risseuw, E., Brogden, D., Zeko, A., Crosby, W.L., Berry,**
747 **C.C., and Ecker, J.R. (2003).** Genome-Wide Insertional Mutagenesis of *Arabidopsis*
748 *thaliana*. *Science* **301**, 653-657.

749 **Atanassov, I., Atanassov, I., Etchells, J.P., and Turner, S. (2009).** A simple, flexible and
750 efficient PCR-fusion/Gateway cloning procedure for gene fusion, site-directed
751 mutagenesis, short sequence insertion and domain deletions and swaps. *Plant Methods*
752 **5**, 14.

753 **Bae, S., Park, J., and Kim, J.-S.** (2014). Cas-OFFinder: a fast and versatile algorithm that
754 searches for potential off-target sites of Cas9 RNA-guided endonucleases.
755 *Bioinformatics* **30**, 1473-1475.

756 **Baima, S., Nobili, F., Sessa, G., Lucchetti, S., Ruberti, I., and Morelli, G.** (1995). The
757 expression of the Athb-8 homeobox gene is restricted to provascular cells in
758 *Arabidopsis thaliana*. *Development* **121**, 4171-4182.

759 **Baima, S., Possenti, M., Matteucci, A., Wisman, E., Altamura, M.M., Ruberti, I., and**
760 **Morelli, G.** (2001). The *Arabidopsis* ATHB-8 HD-Zip Protein Acts as a
761 Differentiation-Promoting Transcription Factor of the Vascular Meristems. *Plant*
762 *Physiology* **126**, 643-655.

763 **Baima, S., Forte, V., Possenti, M., Peñalosa, A., Leoni, G., Salvi, S., Felici, B., Ruberti,**
764 **I., and Morelli, G.** (2014). Negative feedback regulation of auxin signaling by
765 ATHB8/ACL5-BUD2 transcription module. *Molecular plant* **7**, 1006-1025.

766 **Bell, E.M., Lin, W.-c., Husbands, A.Y., Yu, L., Jaganatha, V., Jablonska, B., Mangeon,**
767 **A., Neff, M.M., Girke, T., and Springer, P.S.** (2012). *Arabidopsis* LATERAL
768 ORGAN BOUNDARIES negatively regulates brassinosteroid accumulation to limit
769 growth in organ boundaries. *Proceedings of the National Academy of Sciences* **109**,
770 21146-21151.

771 **Berleth, T., and Jurgens, G.** (1993). The role of the *monopteros* gene in organising the basal
772 body region of the *Arabidopsis* embryo. *Development* **118**, 575-587.

773 **Bolstad, B.M., Irizarry, R.A., Astrand, M., and Speed, T.P.** (2003). A comparison of
774 normalization methods for high density oligonucleotide array data based on variance
775 and bias. *Bioinformatics* **19**, 185-193.

776 **Brackmann, K., Qi, J., Gebert, M., Jouannet, V., Schlamp, T., Grünwald, K., Wallner,**
777 **E.-S., Novikova, D.D., Levitsky, V.G., Agustí, J., Sanchez, P., Lohmann, J.U.,**
778 **and Greb, T.** (2018). Spatial specificity of auxin responses coordinates wood
779 formation. *Nature Communications* **9**, 875.

780 **Brady, S.M., Zhang, L., Megraw, M., Martinez, N.J., Jiang, E., Yi, C.S., Liu, W., Zeng,**
781 **A., Taylor-Teeples, M., Kim, D., Ahnert, S., Ohler, U., Ware, D., Walhout,**
782 **A.J.M., and Benfey, P.N.** (2011). A stele-enriched gene regulatory network in the
783 *Arabidopsis* root. *Mol Syst Biol* **7**.

784 **Cano-Delgado, A., Yin, Y.H., Yu, C., Vafeados, D., Mora-Garcia, S., Cheng, J.C., Nam,**
785 **K.H., Li, J.M., and Chory, J.** (2004). BRL1 and BRL3 are novel brassinosteroid

786 receptors that function in vascular differentiation in Arabidopsis. *Development* **131**,
787 5341-5351.

788 **Carlsbecker, A., Lee, J.-Y., Roberts, C.J., Dettmer, J., Lehesranta, S., Zhou, J.,**
789 **Lindgren, O., Moreno-Risueno, M.A., Vatén, A., Thitamadee, S., Campilho, A.,**
790 **Sebastian, J., Bowman, J.L., Helariutta, Y., and Benfey, P.N.** (2010). Cell
791 signalling by microRNA165/6 directs gene dose-dependent root cell fate. *Nature* **465**,
792 316-321.

793 **Chen, M.-K., Wilson, R.L., Palme, K., Ditengou, F.A., and Shpak, E.D.** (2013). ERECTA
794 Family Genes Regulate Auxin Transport in the Shoot Apical Meristem and Forming
795 Leaf Primordia. *Plant Physiology* **162**, 1978-1991.

796 **Cho, H., Ryu, H., Rho, S., Hill, K., Smith, S., Audenaert, D., Park, J., Han, S.,**
797 **Beeckman, T., Bennett, M.J., Hwang, D., De Smet, I., and Hwang, I.** (2014). A
798 secreted peptide acts on BIN2-mediated phosphorylation of ARFs to potentiate auxin
799 response during lateral root development. *Nat Cell Biol* **16**, 66-76.

800 **Clough, S.J., and Bent, A.F.** (1998). Floral dip: a simplified method for *Agrobacterium*-
801 mediated transformation of *Arabidopsis thaliana*. *Plant Journal* **16**, 735-743.

802 **De Rybel, B., Möller, B., Yoshida, S., Grabowicz, I., Barbier de Reuille, P., Boeren, S.,**
803 **Smith, R.S., Borst, J.W., and Weijers, D.** (2013). A bHLH Complex Controls
804 Embryonic Vascular Tissue Establishment and Indeterminate Growth in Arabidopsis.
805 *Developmental cell*.

806 **De Rybel, B., Adibi, M., Breda, A.S., Wendrich, J.R., Smit, M.E., Novák, O.,**
807 **Yamaguchi, N., Yoshida, S., Van Isterdael, G., Palovaara, J., Nijssse, B.,**
808 **Boekschoten, M.V., Hooiveld, G., Beeckman, T., Wagner, D., Ljung, K., Fleck,**
809 **C., and Weijers, D.** (2014). Integration of growth and patterning during vascular
810 tissue formation in Arabidopsis. *Science (New York, N.Y.)* **345**, 1255215-1255215.

811 **Duarte, P., Ribeiro, D., Carqueijeiro, I., Bettencourt, S., and Sottomayor, M.** (2016).
812 Protoplast Transformation as a Plant-Transferable Transient Expression System. In
813 *Biotechnology of Plant Secondary Metabolism: Methods and Protocols*, A.G. Fett-
814 Neto, ed (New York, NY: Springer New York), pp. 137-148.

815 **Emery, J.F., Floyd, S.K., Alvarez, J., Eshed, Y., Hawker, N.P., Izhaki, A., Baum, S.F.,**
816 **and Bowman, J.L.** (2003). Radial Patterning of *Arabidopsis* Shoots by Class III HD-
817 ZIP and KANADI Genes. *Current Biology* **13**, 1768-1774.

818 **Etchells, J.P., and Turner, S.R.** (2010). The PXY-CLE41 receptor ligand pair defines a
819 multifunctional pathway that controls the rate and orientation of vascular cell division.
820 *Development* **137**, 767-774.

821 **Etchells, J.P., Provost, C.M., and Turner, S.R.** (2012). Plant Vascular Cell Division Is
822 Maintained by an Interaction between PXY and Ethylene Signalling. *PLoS Genetics*
823 **8**, e1002997.

824 **Etchells, J.P., Provost, C.M., Mishra, L., and Turner, S.R.** (2013). *WOX4* and *WOX14* act
825 downstream of the PXY receptor kinase to regulate plant vascular proliferation
826 independently of any role in vascular organisation. *Development* **140**, 2224-2234.

827 **Fischer, U., Kucukoglu, M., Helariutta, Y., and Bhalerao, R.P.** (2019). The Dynamics of
828 Cambial Stem Cell Activity **70**, null.

829 **Fisher, K., and Turner, S.** (2007). PXY, a receptor-like kinase essential for maintaining
830 polarity during plant vascular-tissue development. *Current Biology* **17**, 1061-1066.

831 **Gälweiler, L., Guan, C., Müller, A., Wisman, E., Mendgen, K., Yephremov, A., and**
832 **Palme, K.** (1998). Regulation of Polar Auxin Transport by AtPIN1 in Arabidopsis
833 Vascular Tissue. *Science* **282**, 2226-2230.

834 **Gaudinier, A., Tang, M., Bagman, A.M., and Brady, S.M.** (2017). Identification of
835 Protein-DNA Interactions Using Enhanced Yeast One-Hybrid Assays and a
836 Semiautomated Approach. *Methods Mol Biol* **1610**, 187-215.

837 **Gaudinier, A., Zhang, L., Reece-Hoyes, J.S., Taylor-Teeples, M., Pu, L., Liu, Z., Breton,**
838 **G., Pruneda-Paz, J.L., Kim, D., Kay, S.A., Walhout, A.J.M., Ware, D., and**
839 **Brady, S.M.** (2011). Enhanced Y1H assays for Arabidopsis. *Nat Meth* **8**, 1053-1055.

840 **Guo, Y., Qin, G., Gu, H., and Qu, L.-J.** (2009). Dof5.6/HCA2, a Dof Transcription Factor
841 Gene, Regulates Interfascicular Cambium Formation and Vascular Tissue
842 Development in Arabidopsis. *The Plant Cell*, tpc.108.064139.

843 **Han, S., Cho, H., Noh, J., Qi, J., Jung, H.-J., Nam, H., Lee, S., Hwang, D., Greb, T., and**
844 **Hwang, I.** (2018). BIL1-mediated MP phosphorylation integrates PXY and cytokinin
845 signalling in secondary growth. *Nature Plants*.

846 **Hardtke, C.S., and Berleth, T.** (1998). The Arabidopsis gene MONOPTEROS encodes a
847 transcription factor mediating embryo axis formation and vascular development.
848 *Embo Journal* **17**, 1405-1411.

849 **He, J.-X., Gendron, J.M., Yang, Y., Li, J., and Wang, Z.-Y.** (2002). The GSK3-like kinase
850 BIN2 phosphorylates and destabilizes BZR1, a positive regulator of the

851 brassinosteroid signaling pathway in *Arabidopsis*. Proceedings of the
852 National Academy of Sciences **99**, 10185-10190.

853 **Hellens, R.P., Allan, A.C., Friel, E.N., Bolitho, K., Grafton, K., Templeton, M.D.,**
854 **Karunairetnam, S., Gleave, A.P., and Laing, W.A.J.P.M.** (2005). Transient
855 expression vectors for functional genomics, quantification of promoter activity and
856 RNA silencing in plants **1**, 13.

857 **Hirakawa, Y., Kondo, Y., and Fukuda, H.** (2010). TDIF Peptide Signaling Regulates
858 Vascular Stem Cell Proliferation via the WOX4 Homeobox Gene in *Arabidopsis*.
859 *Plant Cell* **22**, 2618-2629.

860 **Hirakawa, Y., Shinohara, H., Kondo, Y., Inoue, A., Nakanomyo, I., Ogawa, M., Sawa,**
861 **S., Ohashi-Ito, K., Matsubayashi, Y., and Fukuda, H.** (2008). Non-cell-
862 autonomous control of vascular stem cell fate by a CLE peptide/receptor system.
863 *Proceedings of the National Academy of Sciences, USA* **105**, 15208-15213.

864 **Ikematsu, S., Tasaka, M., Torii, K.U., and Uchida, N.** (2017). ERECTA-family receptor
865 kinase genes redundantly prevent premature progression of secondary growth in the
866 *Arabidopsis* hypocotyl. *New Phytologist* **213**, 1697-1709.

867 **Ito, Y., Nakanomyo, I., Motose, H., Iwamoto, K., Sawa, S., Dohmae, N., and Fukuda, H.**
868 (2006). Dodeca-CLE peptides as suppressors of plant stem cell differentiation.
869 *Science* **313**, 842-845.

870 **Iwakawa, H., Ueno, Y., Semiarti, E., Onouchi, H., Kojima, S., Tsukaya, H., Hasebe, M.,**
871 **Soma, T., Ikezaki, M., Machida, C., and Machida, Y.** (2002). The *ASYMMETRIC*
872 *LEAVES 2* gene of *Arabidopsis thaliana*, required for formation of a symmetric flat
873 leaf lamina, encodes a member of a novel family of proteins characterised by cystein
874 repeats and a leucine zipper. *Plant and Cell Physiology* **43**, 467-478.

875 **Ji, J., Strable, J., Shimizu, R., Koenig, D., Sinha, N., and Scanlon, M.J.** (2010). WOX4
876 Promotes Procambial Development. *Plant Physiology* **152**, 1346-1356.

877 **Kalir, S., Mangan, S., and Alon, U.** (2005). A coherent feed-forward loop with a SUM
878 input function prolongs flagella expression in *Escherichia coli* **1**,
879 2005.0006.

880 **Kaplan, S., Bren, A., Dekel, E., and Alon, U.** (2008). The incoherent feed-forward loop
881 can generate non-monotonic input functions for genes **4**, 203.

882 **Kim, T.-W., Michniewicz, M., Bergmann, D.C., and Wang, Z.-Y.** (2012). Brassinosteroid
883 regulates stomatal development by GSK3-mediated inhibition of a MAPK pathway.
884 *Nature* **482**, 419.

885 **Kondo, Y., Ito, T., Nakagami, H., Hirakawa, Y., Saito, M., Tamaki, T., Shirasu, K., and**
886 **Fukuda, H.** (2014). Plant GSK3 proteins regulate xylem cell differentiation
887 downstream of TDIF–TDR signalling. *Nat Commun* **5**.

888 **Konishi, M., Donner, T.J., Scarpella, E., and Yanagisawa, S.** (2015). MONOPTEROS
889 directly activates the auxin-inducible promoter of the Dof5.8 transcription factor gene
890 in *Arabidopsis thaliana* leaf provascular cells. *Journal of Experimental Botany* **66**,
891 283-291.

892 **Laux, T., Mayer, K.F., Berger, J., and Jurgens, G.** (1996). The WUSCHEL gene is
893 required for shoot and floral meristem integrity in *Arabidopsis*. *Development* **122**, 87-
894 96.

895 **Le Hir, R., and Bellini, C.** (2013). The Plant-Specific Dof Transcription Factors Family:
896 New Players Involved in Vascular System Development and Functioning in
897 *Arabidopsis*. *Frontiers in Plant Science* **4**.

898 **Li, C., and Wong, W.H.** (2001). Model-based analysis of oligonucleotide arrays: Expression
899 index computation and outlier detection. *Proceedings of the National Academy of*
900 *Sciences, USA* **98**, 31-36.

901 **Lincoln, C., Britton, J.H., and Estelle, M.** (1990). Growth and development of the *axr1*
902 mutants of *Arabidopsis* **2**, 1071-1080.

903 **Mangan, S., and Alon, U.** (2003). Structure and function of the feed-forward loop network
904 motif. *Proceedings of the National Academy of Sciences* **100**, 11980-11985.

905 **Mattsson, J., Ckurshumova, W., and Berleth, T.** (2003). Auxin signaling in *Arabidopsis*
906 leaf vascular development. *Plant physiology* **131**, 1327-1339.

907 **McConnell, J.R., Emery, J., Eshed, Y., Bao, N., Bowman, J., and Barton, M.K.** (2001).
908 Role of *PHABULOSA* and *PHAVOLUTA* in determining radial patterning in shoots.
909 *Nature* **411**, 709-713.

910 **Mellor, N., Adibi, M., El-Showk, S., De Rybel, B., King, J., Mähönen, A.P., Weijers, D.,**
911 **and Bishopp, A.** (2016). Theoretical approaches to understanding root vascular
912 patterning: a consensus between recent models. *Journal of Experimental Botany*.

913 **Miyashima, S., Roszak, P., Sevilem, I., Toyokura, K., Blob, B., Heo, J.-o., Mellor, N.,**
914 **Help-Rinta-Rahko, H., Otero, S., Smet, W., Boekschoten, M., Hooiveld, G.,**
915 **Hashimoto, K., Smetana, O., Siligato, R., Wallner, E.-S., Mähönen, A.P., Kondo,**
916 **Y., Melnyk, C.W., Greb, T., Nakajima, K., Sozzani, R., Bishopp, A., De Rybel,**
917 **B., and Helariutta, Y.** (2019). Mobile PEAR transcription factors integrate positional
918 cues to prime cambial growth. *Nature*.

919 **Morita, J., Kato, K., Nakane, T., Kondo, Y., Fukuda, H., Nishimasu, H., Ishitani, R.,**
920 **and Nureki, O.** (2016). Crystal structure of the plant receptor-like kinase TDR in
921 complex with the TDIF peptide. *Nature Communications* **7**, 12383.

922 **Müller, C.J., Valdés, A.E., Wang, G., Ramachandran, P., Beste, L., Uddenberg, D., and**
923 **Carlsbecker, A.** (2016). PHABULOSA Mediates an Auxin Signaling Loop to
924 Regulate Vascular Patterning in Arabidopsis. *Plant physiology* **170**, 956-970.

925 **Muraro, D., Mellor, N., Pound, M.P., Help, H., Lucas, M., Chopard, J., Byrne, H.M.,**
926 **Godin, C., Hodgman, T.C., King, J.R., Pridmore, T.P., Helariutta, Y., Bennett,**
927 **M.J., and Bishopp, A.** (2014). Integration of hormonal signaling networks and
928 mobile microRNAs is required for vascular patterning in Arabidopsis roots. *PNAS*
929 **111**, 857-862.

930 **Ohashi-Ito, K., and Bergmann, D.C.** (2007). Regulation of the Arabidopsis root vascular
931 initial population by LONESOME HIGHWAY. *Development* **134**, 2959-2968.

932 **Ohashi-Ito, K., Saegusa, M., Iwamoto, K., Oda, Y., Katayama, H., Kojima, M.,**
933 **Sakakibara, H., and Fukuda, H.** (2014). A bHLH complex activates vascular cell
934 division via cytokinin action in root apical meristem. *Current biology : CB* **24**, 2053-
935 2058.

936 **Okushima, Y., Fukaki, H., Onoda, M., Theologis, A., and Tasaka, M.** (2007). ARF7 and
937 ARF19 Regulate Lateral Root Formation via Direct Activation of LBD/ASL Genes in
938 Arabidopsis. *The Plant Cell* **19**, 118-130.

939 **Peterson, B.A., Haak, D.C., Nishimura, M.T., Teixeira, P.J.P.L., James, S.R., Dangl,**
940 **J.L., and Nimchuk, Z.L.** (2016). Genome-Wide Assessment of Efficiency and
941 Specificity in CRISPR/Cas9 Mediated Multiple Site Targeting in Arabidopsis. *PLOS*
942 *ONE* **11**, e0162169.

943 **Prigge, M.J., Otsuga, D., Alonso, J.M., Ecker, J.R., Drews, G.N., and Clark, S.E.** (2005).
944 Class III homeodomain-leucine zipper gene family members have overlapping,
945 antagonistic, and distinct roles in Arabidopsis development. *Plant Cell* **17**, 61-76.

946 **Ragni, L., Nieminen, K., Pacheco-Villalobos, D., Sibout, R., Schwechheimer, C., and**
947 **Hardtke, C.S.** (2011). Mobile Gibberellin Directly Stimulates Arabidopsis Hypocotyl
948 Xylem Expansion. *Plant Cell* **23**, 1322-1336.

949 **Ramachandran, P., Carlsbecker, A., and Etchells, J.P.** (2016). Class III HD-ZIPs govern
950 vascular cell fate: an HD view on patterning and differentiation. *Journal of*
951 *Experimental Botany*.

952 **Ramakers, C., Ruijter, J.M., Deprez, R.H.L., and Moorman, A.F.M.** (2003).
953 Assumption-free analysis of quantitative real-time polymerase chain reaction (PCR)
954 data. *Neuroscience Letters* **339**, 62-66.

955 **Reece-Hoyes, J.S., Diallo, A., Lajoie, B., Kent, A., Shrestha, S., Kadreppa, S., Pesyna,**
956 **C., Dekker, J., Myers, C.L., and Walhout, A.J.M.** (2011). Enhanced yeast one-
957 hybrid assays for high-throughput gene-centered regulatory network mapping. *Nature*
958 *Methods* **8**, 1059.

959 **Ruonala, R., Ko, D., and Helariutta, Y.** (2017). Genetic Networks in Plant Vascular
960 Development **51**, 335-359.

961 **Sachs, T.** (1969). Polarity and the Induction of Organized Vascular Tissues. *Annals of*
962 *Botany* **33**, 263-275.

963 **Sarkar, A.K., Luijten, M., Miyashima, S., Lenhard, M., Hashimoto, T., Nakajima, K.,**
964 **Scheres, B., Heidstra, R., and Laux, T.** (2007). Conserved factors regulate
965 signalling in *Arabidopsis thaliana* shoot and root stem cell organizers. *Nature* **446**,
966 811-814.

967 **Schlereth, A., Moller, B., Liu, W., Kientz, M., Flipse, J., Rademacher, E.H., Schmid, M.,**
968 **Jurgens, G., and Weijers, D.** (2010). MONOPTEROS controls embryonic root
969 initiation by regulating a mobile transcription factor. *Nature* **464**, 913-916.

970 **Shannon, P., Markiel, A., Ozier, O., Baliga, N.S., Wang, J.T., Ramage, D., Amin, N.,**
971 **Schwikowski, B., and Ideker, T.** (2003). Cytoscape: A Software Environment for
972 Integrated Models of Biomolecular Interaction Networks. *Genome Research* **13**,
973 2498-2504.

974 **Shen-Orr, S.S., Milo, R., Mangan, S., and Alon, U.** (2002). Network motifs in the
975 transcriptional regulation network of *Escherichia coli*. *Nature Genetics* **31**, 64.

976 **Shuai, B., Reynaga-Peña, C.G., and Springer, P.S.** (2002). The Lateral Organ Boundaries
977 Gene Defines a Novel, Plant-Specific Gene Family. *Plant Physiology* **129**, 747-761.

978 **Smet, W., Sevilem, I., de Luis Balaguer, M.A., Wybouw, B., Mor, E., Miyashima, S.,**
979 **Blob, B., Roszak, P., Jacobs, T.B., Boekschoten, M., Hooiveld, G., Sozzani, R.,**
980 **Helariutta, Y., and De Rybel, B.** (2019). DOF2.1 Controls Cytokinin-Dependent
981 Vascular Cell Proliferation Downstream of TMO5/LHW. *Current Biology* **29**, 520-
982 529.e526.

983 **Smetana, O., Mäkilä, R., Lyu, M., Amiryousefi, A., Sánchez Rodríguez, F., Wu, M.-F.,**
984 **Solé-Gil, A., Leal Gavarrón, M., Siligato, R., Miyashima, S., Roszak, P.,**
985 **Blomster, T., Reed, J.W., Broholm, S., and Mähönen, A.P.** (2019). High levels of

986 auxin signalling define the stem-cell organizer of the vascular cambium. *Nature* **565**,
987 485-489.

988 **Smyth, G.K.** (2004). Linear Models and Empirical Bayes Methods for Assessing Differential
989 Expression in Microarray Experiments. *Statistical Applications in Genetics and*
990 *Molecular Biology* **3**, Article 3.

991 **Suer, S., Agusti, J., Sanchez, P., Schwarz, M., and Greb, T.** (2011). WOX4 Imparts Auxin
992 Responsiveness to Cambium Cells in Arabidopsis. *The Plant Cell* **23**, 3247-3259.

993 **Sun, C.N.** (1955). Anomalous Structure in the Hypocotyl of Soybean Following Treatment
994 with 2,4-Dichlorophenoxyacetic Acid **121**, 641-641.

995 **Swarbreck, D., Wilks, C., Lamesch, P., Berardini, T.Z., Garcia-Hernandez, M.,**
996 **Foerster, H., Li, D., Meyer, T., Muller, R., Ploetz, L., Radenbaugh, A., Singh, S.,**
997 **Swing, V., Tissier, C., Zhang, P., and Huala, E.** (2008). The Arabidopsis
998 Information Resource (TAIR): gene structure and function annotation. *Nucl. Acids*
999 *Res.* **36**, D1009-1014.

1000 **Taylor-Teeple, M., Lin, L., de Lucas, M., Turco, G., Toal, T.W., Gaudinier, A., Young,**
1001 **N.F., Trabucco, G.M., Veling, M.T., Lamothe, R., Handakumbura, P.P., Xiong,**
1002 **G., Wang, C., Corwin, J., Tsoukalas, A., Zhang, L., Ware, D., Pauly, M.,**
1003 **Kliebenstein, D.J., Dehesh, K., Tagkopoulos, I., Breton, G., Pruneda-Paz, J.L.,**
1004 **Ahnert, S.E., Kay, S.A., Hazen, S.P., and Brady, S.M.** (2015). An Arabidopsis
1005 gene regulatory network for secondary cell wall synthesis. *Nature* **517**, 571-U307.

1006 **Torrey, J.G.** (1953). THE EFFECT OF CERTAIN METABOLIC INHIBITORS ON
1007 VASCULAR TISSUE DIFFERENTIATION IN ISOLATED PEA ROOTS **40**, 525-
1008 533.

1009 **Uchida, N., and Tasaka, M.** (2013). Regulation of plant vascular stem cells by endodermis-
1010 derived EPFL-family peptide hormones and phloem-expressed ERECTA-family
1011 receptor kinases. *Journal of Experimental Botany*.

1012 **Uchida, N., Lee, J.S., Horst, R.J., Lai, H.-H., Kajita, R., Kakimoto, T., Tasaka, M., and**
1013 **Torii, K.U.** (2012). Regulation of inflorescence architecture by intertissue layer
1014 ligand–receptor communication between endodermis and phloem. *Proc Natl Acad Sci*
1015 *USA*.

1016 **Vera-Sirera, F., De Rybel, B., Úrbez, C., Kouklas, E., Pesquera, M., Álvarez-Mahecha,**
1017 **J.C., Minguet, E.G., Tuominen, H., Carbonell, J., Borst, J.W., Weijers, D., and**
1018 **Blázquez, M.A.** (2015). A bHLH-Based Feedback Loop Restricts Vascular Cell
1019 Proliferation in Plants. *Developmental cell* **35**, 432-443.

1020 **Waki, T., Miyashima, S., Nakanishi, M., Ikeda, Y., Hashimoto, T., and Nakajima, K.**
1021 (2013). A GAL4-based targeted activation tagging system in *Arabidopsis thaliana*.
1022 *The Plant Journal* **73**, 357-367.

1023 **Wang, N., Bagdassarian, K.S., Doherty, R.E., Wang, X.Y., Kroon, J.T., Wang, W.,**
1024 **Jermyn, I.H., Turner, S.R., and Etchells, P.** (2018). Paralogues of the PXY and ER
1025 receptor kinases enforce radial patterning in plant vascular tissue. bioRxiv.

1026 **Wang, N., Bagdassarian, K.S., Doherty, R.E., Kroon, J.T., Connor, K.A., Wang, X.Y.,**
1027 **Wang, W., Jermyn, I.H., Turner, S.R., and Etchells, J.P.** (2019). Organ-specific
1028 genetic interactions between paralogues of the *PXY* and *ER* receptor kinases enforce
1029 radial patterning in *Arabidopsis* vascular tissue. *Development* **146**, dev177105.

1030 **Wang, Z.-P., Xing, H.-L., Dong, L., Zhang, H.-Y., Han, C.-Y., Wang, X.-C., and Chen,**
1031 **Q.-J.** (2015). Egg cell-specific promoter-controlled CRISPR/Cas9 efficiently
1032 generates homozygous mutants for multiple target genes in *Arabidopsis* in a single
1033 generation. *Genome Biology* **16**, 144.

1034 **Woodward, C., Bemis, S.M., Hill, E.J., Sawa, S., Koshiba, T., and Torii, K.U.** (2005).
1035 Interaction of Auxin and ERECTA in Elaborating *Arabidopsis* Inflorescence
1036 Architecture Revealed by the Activation Tagging of a New Member of the YUCCA
1037 Family Putative Flavin Monooxygenases. *Plant Physiology* **139**, 192-203.

1038 **Woody, S., Austin-Phillips, S., Amasino, R., and Krysan, P.** (2007). The WiscDsLox T-
1039 DNA collection: an *Arabidopsis* community resource generated by using an improved
1040 high-throughput T-DNA sequencing pipeline. *Journal of Plant Research* **120**, 157-
1041 165.

1042 **Xing, H.-L., Dong, L., Wang, Z.-P., Zhang, H.-Y., Han, C.-Y., Liu, B., Wang, X.-C., and**
1043 **Chen, Q.-J.** (2014). A CRISPR/Cas9 toolkit for multiplex genome editing in plants.
1044 *BMC Plant Biology* **14**, 327.

1045 **Yoo, S.-D., Cho, Y.-H., and Sheen, J.** (2007). *Arabidopsis* mesophyll protoplasts: a versatile
1046 cell system for transient gene expression analysis. *Nature Protocols* **2**, 1565.

1047 **Yordanov, Y.S., Regan, S., and Busov, V.** (2010). Members of the LATERAL ORGAN
1048 BOUNDARIES DOMAIN Transcription Factor Family Are Involved in the
1049 Regulation of Secondary Growth in *Populus*. *The Plant Cell Online* **22**, 3662-3677.

1050 **Zhang, H., Lin, X., Han, Z., Qu, L.-J., and Chai, J.** (2016). Crystal structure of PXY-TDIF
1051 complex reveals a conserved recognition mechanism among CLE peptide-receptor
1052 pairs. *Cell Research* **26**, 543.

1053 **Zhang, J., Eswaran, G., Alonso-Serra, J., Kucukoglu, M., Xiang, J., Yang, W., Elo, A.,**
1054 **Nieminen, K., Damén, T., Joung, J.-G., Yun, J.-Y., Lee, J.-H., Ragni, L., Barbier**
1055 **de Reuille, P., Ahnert, S.E., Lee, J.-Y., Mähönen, A.P., and Helariutta, Y. (2019).**
1056 **Transcriptional regulatory framework for vascular cambium development in**
1057 **Arabidopsis roots. Nature Plants 5, 1033-1042.**

1058 **Zhong, R., and Ye, Z.-H. (1999). IFL1, a Gene Regulating Interfascicular Fiber**
1059 **Differentiation in Arabidopsis, Encodes a Homeodomain-Leucine Zipper Protein.**
1060 **Plant Cell 11, 2139-2152.**

1061 **Zhong, R., Taylor, J.J., and Ye, Z.H. (1997). Disruption of Interfascicular Fiber**
1062 **Differentiation in an Arabidopsis Mutant. Plant Cell 9, 2159-2170.**

1063

1064

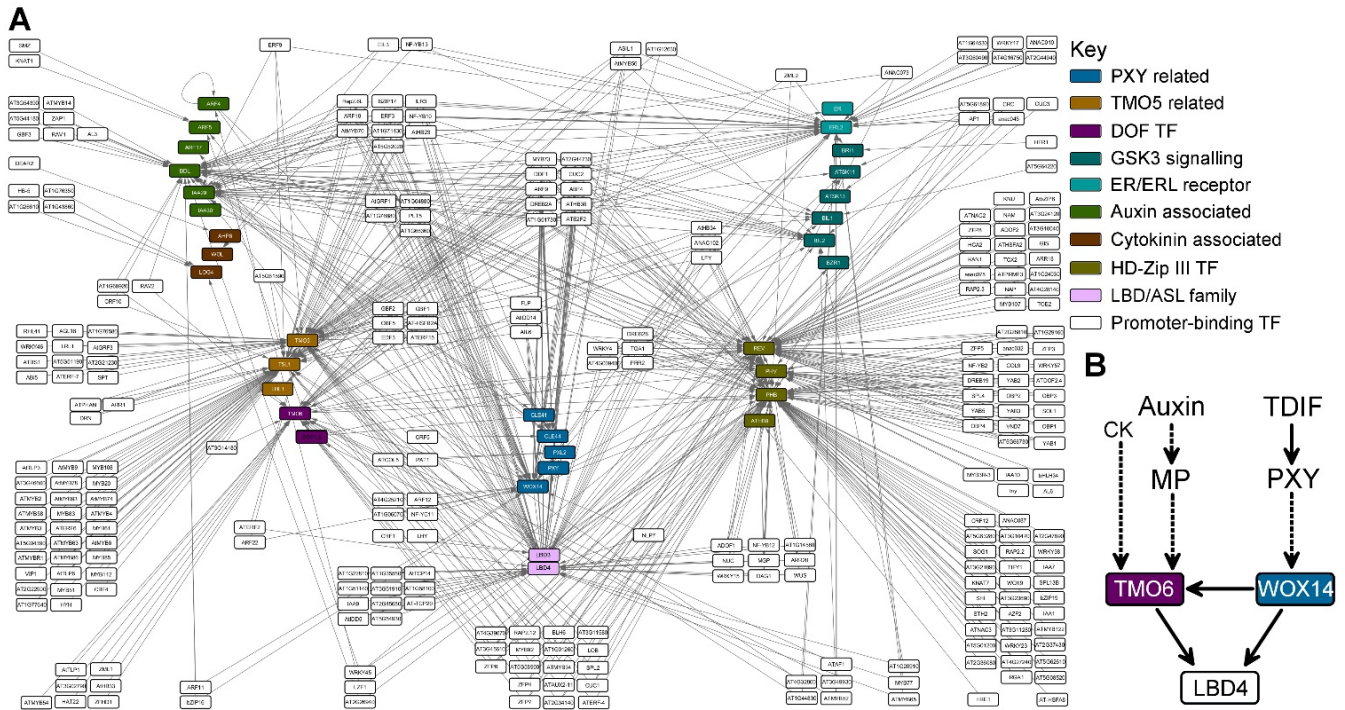


Figure 1. Diagrammatic representation of the vascular development transcriptional regulatory network

(A) Representation of all the interactions identified using eY1H. Promoters screened are shown as coloured nodes. Transcription factors are shown as white nodes. Grey lines connect transcription factor nodes, with promoter nodes representing interactions in eY1H assays. (B) Sub-network describing the feed-forward loop constituted of WOX14, TMO6 and LBD4 interactions, and its regulation by auxin, cytokinin (CK) and TDIF-PXY signalling.

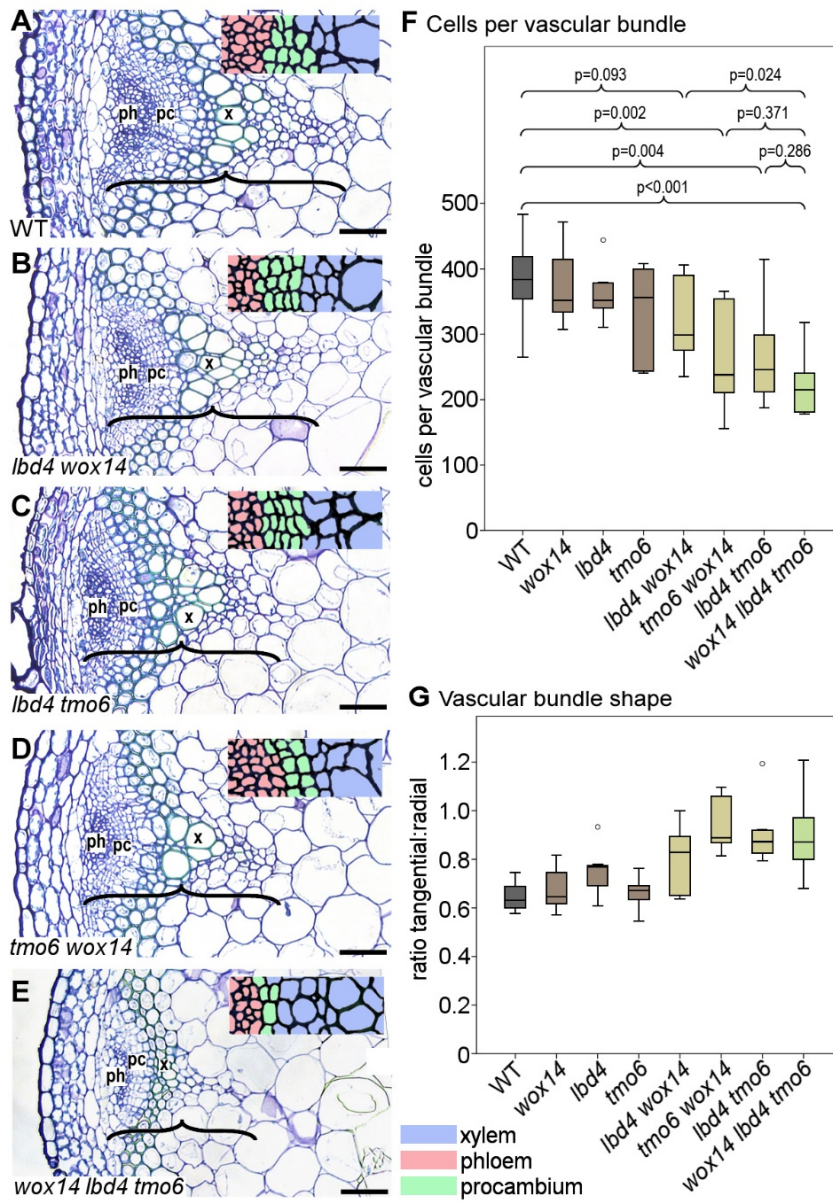


Figure 2. Consequences of removing the feed-forward loop

(A) Morphology of vascular bundles from inflorescence stems. (A) wild type, (B) *lbd4 wox14* (C) *lbd4 tmo6*, (D) *tmo6 wox14*, (E) *wox14 lbd4 tmo6*. Transverse sections were stained with toluidine blue. Insets show close-up of the cambium (green). (F) Boxplots showing mean number of cells per vascular bundle in *wox14 lbd4 tmo6*, double and single mutant controls. Significant differences were determined by ANOVA with an LSD post-hoc test (n=6). (G) Box plot showing vascular bundle shape determined by measuring the ratio of tangential to radial axis (n=6). Scale bars are 50 μ m. x marks xylem, pc marks cambium, ph marks phloem, brackets mark the vascular bundle size along the radial axis of the stem. Boxplots show median (inner line) and inner quartiles (IQ, box). Whiskers extend to the highest and lowest values no greater than 1.5 times the IQ range, circles show outliers.

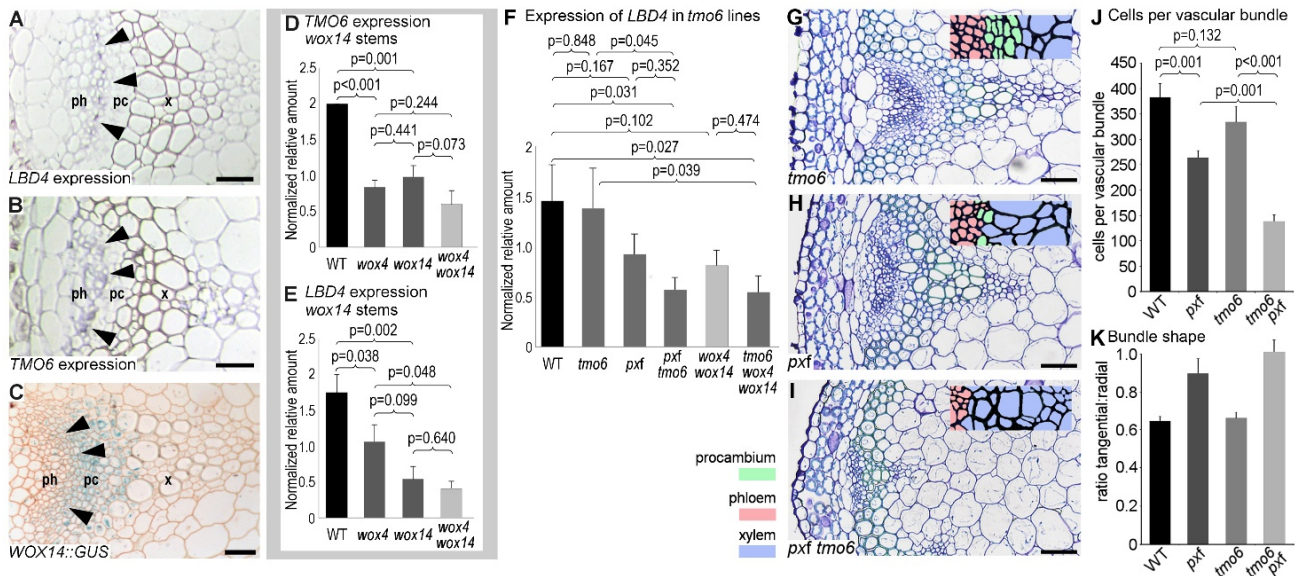


Figure 3. Gene expression studies supporting a regulatory relationship between *WOX14*, *TMO6* and *LBD4*

(A-C) *WOX14*, *TMO6* and *LBD4* demonstrate overlapping expression in inflorescence stem vascular bundles. Antisense probes against *LBD4* mRNA (A) or *TMO6* mRNA (B) localise to the phloem-procambium boundary. (C) *WOX14::GUS* transcriptional fusion showing the presence of broad *WOX14* expression in vascular bundles including at the phloem-procambium boundary (x marks xylem, pc marks cambium, ph marks phloem). (D-E) qRT-PCR on inflorescence stem tissue from the lower third of the stem showing that *TMO6* (D) and *LBD4* (E) expression is dependent on *WOX14*. (F) qRT-PCR showing that *TMO6* and *PXf* are required to maintain *LBD4* expression in the lower half of 15 cm inflorescence stems. Expression differences were determined in technical triplicate for each of three biological replicates. Tissue for each biological replicate was taken from a different pot. Statistical differences were determined with ANOVA and an LSD post-hoc test (n=3 biological replicates; error bars are standard error). (G-I) Vascular bundles from the inflorescence stems of *tmo6* (G), *pxy pxl1 pxl2 (pxf)* (H), and *pxf tmo6* (I) plants. Transverse sections were stained with toluidine blue. Scale bars are 30 μ m. (J) Graph showing mean number of cells per vascular bundle. p values were determined with ANOVA and an LSD post-hoc test. (K) Histogram showing vascular bundle shape determined by measuring the ratio of tangential to radial axis. (n=6; error bars show standard error).

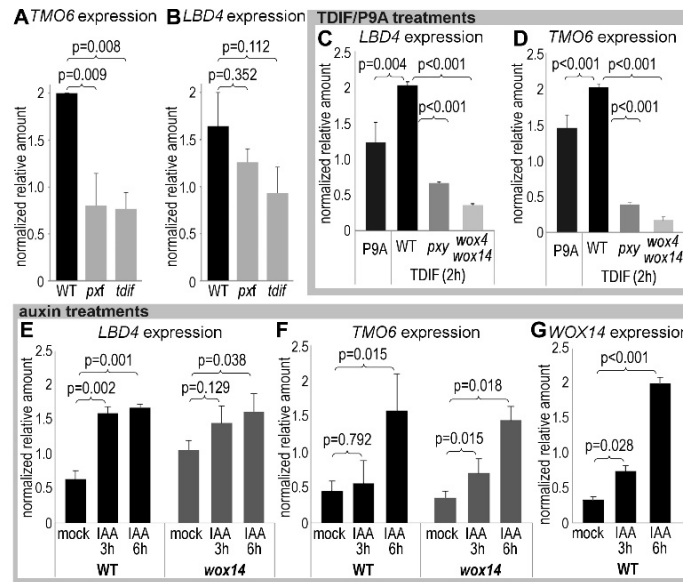


Figure 4. PXY and auxin signalling regulate the feed-forward loop

(A-B) qRT-PCR showing *TMO6* (A) and *LBD4* (B) expression in *pxf* and *tdif* lines. (C-D) *LBD4* (C) or *TMO6* (D) expression in seedlings treated with TDIF or P9A for 2 hours. (E-G) qRT-PCR showing *LBD4* (E), *TMO6* (F), and *WOX14* (G) expression in seedlings treated with IAA for 3 or 6 hours. Expression differences were determined in technical triplicate for each of three biological replicates. Tissue for each biological replicate was taken from a different plate. p values marked on critical comparisons were determined using ANOVA and an LSD post-hoc test ($n=3$ biological replicates; error bars are standard error). Bars show standard error; ANOVA with an LSD post-hoc test ($n=3$ pools).

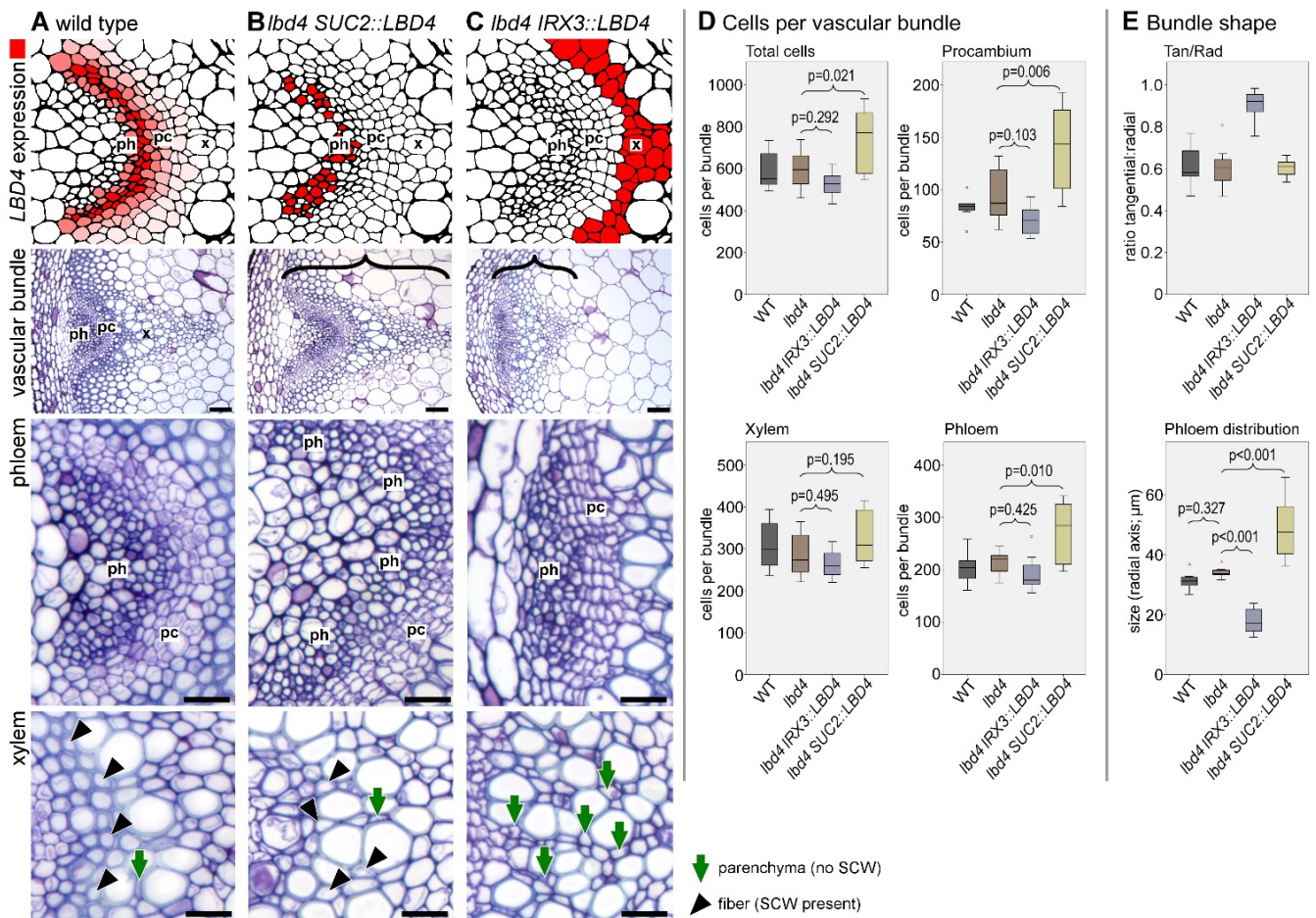


Figure 5. *LBD4* expression patterns the vascular tissue.

(A-C) Consequences of *LBD4* expression at the phloem-procambium boundary (A), in phloem (B), or in xylem (C) in inflorescence stems. Upper panels show diagrammatic representation of the *LBD4* expression domain with subsequent panels showing overall vascular morphology, phloem, and xylem. (A) Wild-type vascular bundle showing an arc of phloem cells, procambium cells and xylem cells along the radial axis of a stem transverse section. Xylem is characterised by the presence of fiber cells with large secondary cell walls (black arrowheads). (B) *lbd4 SUC2::LBD4* lines have an increase phloem size. Xylem fibre cells retain secondary cell walls (black arrowheads). Parenchyma, with no secondary cell wall is marked with a green arrow. (C) *lbd4 IRX3::LBD4* lines demonstrate a change to phloem morphology, as the characteristic arc is absent. Cells where fibres were observed in wild type xylem do not have large secondary cell walls (parenchyma; green arrows). ph is phloem, pc procambium, x is xylem, SCW is secondary cell wall. Scale bars are 50 μM (whole vascular bundle) or 20 μM (xylem and phloem close-ups). The radial axis is marked in (B) and (C) with a black bracket. (D) Boxplots showing the mean number of total cells per vascular bundle (upper left), number of procambium (upper right), phloem (lower right), and xylem (lower left) cells per vascular bundle. p values were determined using ANOVA with an LSD post-hoc test ($n=7$). (E) Upper boxplot shows vascular bundle shape determined by measuring the ratio of the tangential to radial axis, lower boxplot showing distribution of phloem along the radial axis of the stem. p values were determined using ANOVA with an LSD post-hoc test ($n=7$). Boxplots show median (inner line) and inner quartiles (IQ, box). Whiskers extend to the highest and lowest values no greater than 1.5 times the IQ range, circles show outliers.

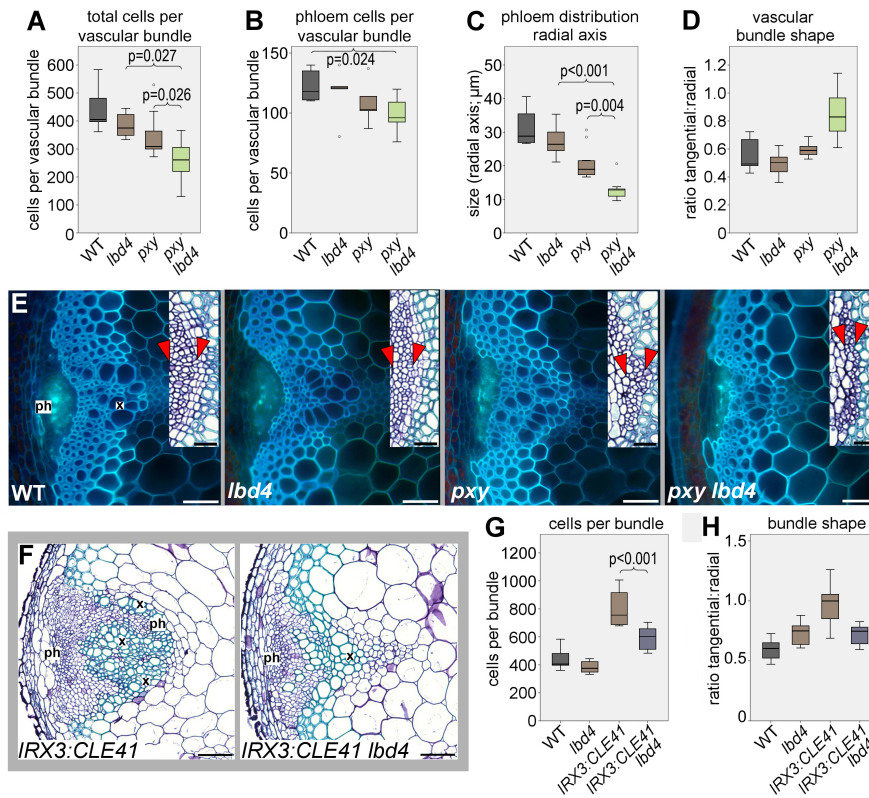


Figure 6. Genetic interactions between *LBD4* and *TDIF-PXY*.

(A-E) Analysis of *pxy lbd4* double mutants and controls. Boxplots showing the total number of cells (A; n=7), number of phloem cells (B; n=6) per vascular bundle in 8-week-old inflorescence stems. (C) Boxplot showing distribution of phloem along the radial axis of the stem (distribution is shown on insets in (E) as tissue between the red arrowheads; n=7). (D) Boxplot showing vascular bundle shape determined by measuring the ratio of the tangential to radial axis (n=8). (E) Aniline blue stained transverse sections of wild type, *lbd4*, *pxy*, *pxy lbd4*. Insets show close up of phloem tissue stained with toluidine blue. (F-H) *lbd4* suppresses *CLE41* misexpression phenotypes. (F) *IRX3:CLE41* vascular bundles are characterised by organisation defects but these defects are attenuated in *IRX3:CLE41 lbd4* lines. Boxplots showing number of cells per vascular bundle, and vascular bundle shape determined by measuring the ratio of tangential to radial axis (n=6). 8-week-old plants were used. Scale bars are 50 μm , except for insets in (D) where scale bars are 20 μm . Bars show standard error; p values in (A-D) and (G) were determined using ANOVA with an LSD post-hoc test. ph is phloem, pc procambium, x is xylem. Boxplots show median (inner line) and inner quartiles (IQ, box). Whiskers extend to the highest and lowest values no greater than 1.5 times the IQ range, circles show outliers.